Redox Biology 70 (2024) 103066

Contents lists available at ScienceDirect

Redox Biology

journal homepage: www.elsevier.com/locate/redox

Hydrogen sulfide protects cardiomyocytes from doxorubicin-induced ferroptosis through the SLC7A11/GSH/GPx4 pathway by Keap1 S-sulfhydration and Nrf2 activation

Hui Zhang [a,c,1], Jianan Pan [a,1], Shuying Huang [a,1], Xiaonan Chen [a], Alex Chia Yu Chang [a,b], Changqian Wang [a], Junfeng Zhang [a,**], Huili Zhang [a,*]

[a] Department of Cardiology, Shanghai Ninth People's Hospital, Shanghai Jiao Tong University School of Medicine, Shanghai, China
[b] Shanghai Institute of Precision Medicine, Shanghai Ninth People's Hospital, Shanghai Jiao Tong University School of Medicine, Shanghai, China
[c] Department of Echocardiography, Zhongshan Hospital, Fudan University, Shanghai Institute of Cardiovascular Diseases, Shanghai Institute of Medical Imaging, Shanghai, China

ARTICLE INFO

Keywords:
Doxorubicin-induced cardiotoxicity
Hydrogen sulfide
Ferroptosis
SLC7A11
S-sulfhydrated Keap1

ABSTRACT

Recent studies have demonstrated that ferroptosis, a novel form of nonapoptotic regulated cell death plays an important role in doxorubicin (DOX)-induced cardiotoxicity (DoIC). Hydrogen sulfide (H_2S) is emerging as the third important gaseous mediator in cardiovascular system. However, whether H_2S has an effect on DOX-induced ferroptosis remains unknown. Here, we found that DOX not only triggered cardiomyocyte ferroptosis but also significantly inhibited the synthesis of endogenous H_2S in the murine model of chronic DoIC. Application of NaHS, an H_2S donor obviously activated the SLC7A11/GSH/GPx4 antioxidant pathway and thus alleviated DOX-induced ferroptosis and cardiac injury in mice. In contrast, cardiac-specific knockout of cystathionine γ-lyase gene (*Cse*) in mice ($Cse^{f/f}$/Cre^{+}) to abolish the cardiac synthesis of endogenous H_2S evidently exacerbated DOX-induced ferroptosis and cardiac dysfunction. A further suppression of SLC7A11/GSH/GPx4 pathway was obtained in $Cse^{f/f}$/Cre^{+} mice with DoIC, as compared to $Cse^{f/f}$/Cre^{-} mice with DoIC. The aggravation caused by cardiac-specific *Cse* deficiency was remarkably rescued by exogenous supplementation of NaHS. Moreover, in DOX-stimulated H9c2 cardiomyocytes, pretreatment with NaHS dose-dependently enhanced the activity of SLC7A11/GSH/GPx4 pathway and subsequently mitigated ferroptosis and mitochondrial impairment. On the contrary, transfection with *Cse* siRNA in DOX-stimulated H9c2 cardiomyocytes markedly inhibited SLC7A11/GSH/GPx4 pathway, thus leading to aggravated ferroptosis and more damage to mitochondrial structure and function. In addition, the protective effect of NaHS on DOX-induced ferroptosis was closely related to the S-sulfhydrated Keap1, which in turn promoted nuclear translocation of Nrf2 and the transcription of SLC7A11 and GPx4. In conclusion, our findings suggest that H_2S may exert protective effect on DoIC by inhibiting DOX-induced ferroptosis via Keap1/Nrf2-dependent SLC7A11/GSH/GPx4 antioxidant pathway.

1. Introduction

Doxorubicin (DOX), as an anthracycline is a potent chemotherapeutic agent used for the treatment of solid tumors and hematological malignancies. However, doxorubicin (DOX)-induced cardiotoxicity (DoIC) including acute left ventricular dysfunction, late-onset cardiomyopathy and heart failure (HF) is still an important health concern [1–3]. Despite extensive effort to explore the mechanisms underlying DoIC, the molecular pathogenesis remains elusive. One major source of cardiomyocyte damage is excessive production of reactive oxygen species (ROS), which harm lipids, DNA or proteins [4]. Topoisomerase II-β-mediated DNA double strand breakage and mitochondrial

* Corresponding author. Department of Cardiology, Shanghai Ninth People's Hospital, Shanghai Jiao Tong University School of Medicine, 639 Zhizaoju Road, Shanghai, 200011, China.
** Corresponding author. Department of Cardiology, Shanghai Ninth People's Hospital, Shanghai Jiao Tong University School of Medicine, 639 Zhizaoju Road, Shanghai, 200011, China.
E-mail addresses: jfzhang_dr@163.com (J. Zhang), huilizhang815@163.com (H. Zhang).
[1] These authors contributed equally to this work.

https://doi.org/10.1016/j.redox.2024.103066
Received 21 January 2024; Received in revised form 28 January 2024; Accepted 28 January 2024
Available online 29 January 2024

damage are also involved in DOX cardiotoxicity [5].

Recently, ferroptosis, a novel regulated cell death (RCD) characterized by the iron-dependent accumulation of lipid peroxides, has been identified to play an important role in DoIC [6]. DOX and its metabolites upregulated transferrin receptor and inactivated ferritin, resulting in disruption of iron homeostasis and iron overload [6,7]. On the other hand, DOX also inhibited the levels of antioxidant substances, including glutathione peroxidase 4 (GPx4), a core regulatory protein to prevent cells from ferroptosis by eliminating intracellular lipid peroxides, as well as SOD and GSH [8]. Lately, Fang et al. found that ferrostatin-1 (Fer-1, an inhibitor of ferroptosis), but not emricasan (an inhibitor of apoptosis), necrostatin-1 (a specific inhibitor of necroptosis) and 3-methyladenine (an inhibitor of autophagy), reduced DOX-induced cardiomyopathy and mortality in mice [9]. Dexrazoxane, the only FDA approved drug to prevent DOX-induced cardiotoxicity in cancer patients, inhibited DOX-induced ferroptosis by chelating iron in cardiomyocytes [10]. These findings highlight the importance of ferroptosis in the pathology of DoIC and suggest that ferroptosis may be a promising target for the prevention of DoIC.

Hydrogen sulfide (H_2S) is endogenously synthesized from L-cysteine by several enzymes, including cystathionine-γ-lyase (CSE), cystathionine-β-synthase (CBS), 3-mercaptopyruvate sulfurtransferase (3-MPST) and cysteine aminotransferase (CAT) [11]. H_2S has long been regarded as toxic gas because of its ability to inhibit the activity of cytochrome *c* oxidase and destroy mitochondrial respiration [12]. However, its toxicological profiles mainly depend on the exposure concentrations [12]. Growing evidences show that H_2S endogenously produced in mammalian cells at a very low level exerts various biological functions. It combats oxidative species, reacts with the metal centers of iron-heme proteins, and modifies protein cysteine residues known as persulfidation [13–15]. The interaction of H_2S with various signaling molecules has been suggested to aid in signaling transduction and play important role in cardiovascular diseases, including atherosclerosis, coronary heart disease, heart failure, hypertension, pulmonary arterial hypertension, and myocardial ischemia/reperfusion injury [16–20]. Although H_2S has been shown to confer protection against DoIC [21–25], it is unclear whether H_2S is involved in the pathogenesis of DOX-induced ferroptosis.

It is well established that H_2S is critical for maintaining balanced amounts of antioxidants in the body [12]. Appropriate levels of H_2S shield cardiomyocytes from oxidative stress by directly scavenging ROS and reactive nitrogen species (RNS), reducing glutathione disulfide (GSSG) and enhancing the level of glutathione (GSH) [12,26]. Hence, we speculated that H_2S is likely to have an effective role in repressing DOX-induced ferroptosis. Unfortunately, how H_2S could affect ferroptosis in DoIC and the underlying mechanism are rarely investigated. Therefore, the present study was designed to examine the role and the mechanism of H_2S in DOX-induced ferroptosis in cardiomyocytes. Our findings suggest that H_2S combated DOX-induced ferroptosis and cardiac injury by upregulating the activity of the lipid peroxide repair system, solute carrier family 7-member 11-glutathione (SLC7A11)/GSH/GPx4 pathway [10,27] through inducing Kelch-like ECH-Associating protein 1(Keap1) S-sulfhydration and activating Nuclear Erythroid 2-Related Factor 2 (Nrf2) [28,29], but having no effect on iron overload.

2. Materials and methods

2.1. Animal experiments

The current study was ethically carried out in strict accordance with the recommendations of the "Guide for the Care and Use of Laboratory Animals" and the protocol was approved by the Animal Experiment Ethics Committee of Shanghai Jiao Tong University School of Medicine. Male 7-week-old C57BL/6J mice weighing 18–20 g were purchased from Shanghai Model Organisms Center (Shanghai, China) and housed in a standard raising condition of controlled humidity and a 12-h day/night cycle at 22 °C. After 1 week of the acclimation period, the animals were randomly given DOX (i.p., 5 mg/kg/week; Cat#HY-15142, MedChemExpress, USA) or saline for 4 weeks. During the DOX injection, mice were administered with NaHS (an H_2S donor; i.p., 1 mg/kg/day; Cat#LS7485, Macklin, China), Ferrostatin-1 (Fer-1, a lipid peroxidation cleaner; i.p., 2 μmol/kg/day; Cat#100579, MedChemExpress, USA) or saline. To inhibit the production of endogenous H_2S in cardiomyocytes, *Cse*-floxed mice on a C57BL/6J background were generated using a LoxP-targeting system at the Shanghai Model Organisms Center. The *Cse*-floxed mice were crossed with cardiac-specific and tamoxifen-inducible *Myh6*-cre transgenic mice (Cre-ERT2, Cre recombinase fused to a mutant estrogen ligand-binding domain) to obtain age matched $Cse^{f/f}/cre^{-}$ and $Cse^{f/f}/cre^{+}$ mice for experiments. 2 weeks before DOX treatment, both $Cse^{f/f}/cre^{-}$ and $Cse^{f/f}/cre^{+}$ mice were administered Tamoxifen (i.p., 75 mg/kg/day; Cat#HY-13757A, MedChemExpress, USA) for a total of 5 consecutive days for cre characterization work. 2 weeks after the last injection of DOX, echocardiography was implemented, blood samples and heart tissues were obtained from mice euthanized using deep isoflurane (5 %) anesthesia and stored at −80 °C for subsequent use. The experimental design paradigm was shown in Fig. S1.

2.2. Echocardiography

Transthoracic echocardiography was performed using a 30-MHz high-frequency scan probe (Vevo 2100, VisualSonics, Canada). Mice were anesthetized and maintained under 1–3 % isoflurane and 2 L/min 100 % oxygen during the procedure. Echocardiographic measurements were performed by a blinded investigator as previously described [30]. Left ventricular ejection fraction (EF) and fractional shortening (FS) were measured and calculated using Vevo Analysis software.

2.3. Histological analysis

The heart tissues were fixed with 4 % paraformaldehyde and embedded in paraffin. The paraffin-embedded hearts were then sectioned and stained with hematoxylin-eosin (Cat#G1005, Servicebio Biotech, China) and Masson trichrome staining reagent (Cat#G1006, Servicebio Biotech, China) according to the manufacturer's instructions. The images were observed and captured with Nikon Eclipse Ti fluorescence microscope (Nikon, Japan) and processed with Image J software.

2.4. Immunohistochemistry

The heart sections were deparaffinized and rehydrated by gradient elution using xylene and ethanol, followed by washing with phosphate-buffered saline (PBS). To quench endogenous peroxidase activity, heart sections were incubated with peroxidase blocking reagent (3 % H_2O_2 in methanol) for 10 min. Prepared heart sections were blocked by incubation with 5 % goat serum (Cat#C0265, Beyotime Biotechnology, China) for 1 h at 37 °C, and then incubated overnight with primary antibodies (Table S1) at 4 °C under humidified conditions, followed by incubation for 1 h with HRP conjugated anti-rabbit secondary antibody (Cat#GB23303, 1:500, Servicebio Biotech, China) at room temperature. Control slides stained with isotype IgG controls were prepared to determine the antibody specificity of each staining. After washing with PBS, the DAB Solution was used to cover the entire tissue section and incubate for 5 min. Stained slides were observed using Nikon Eclipse Ti fluorescence microscope (Nikon, Japan) and analyzed using Image J software.

2.5. Measurement of plasma H_2S

120 μL aliquots of plasma were mixed with 100 μL distilled water and 60 μL 1 % zinc acetate to trap H_2S. Subsequently, 40 μL N, N-dimethyl-p-

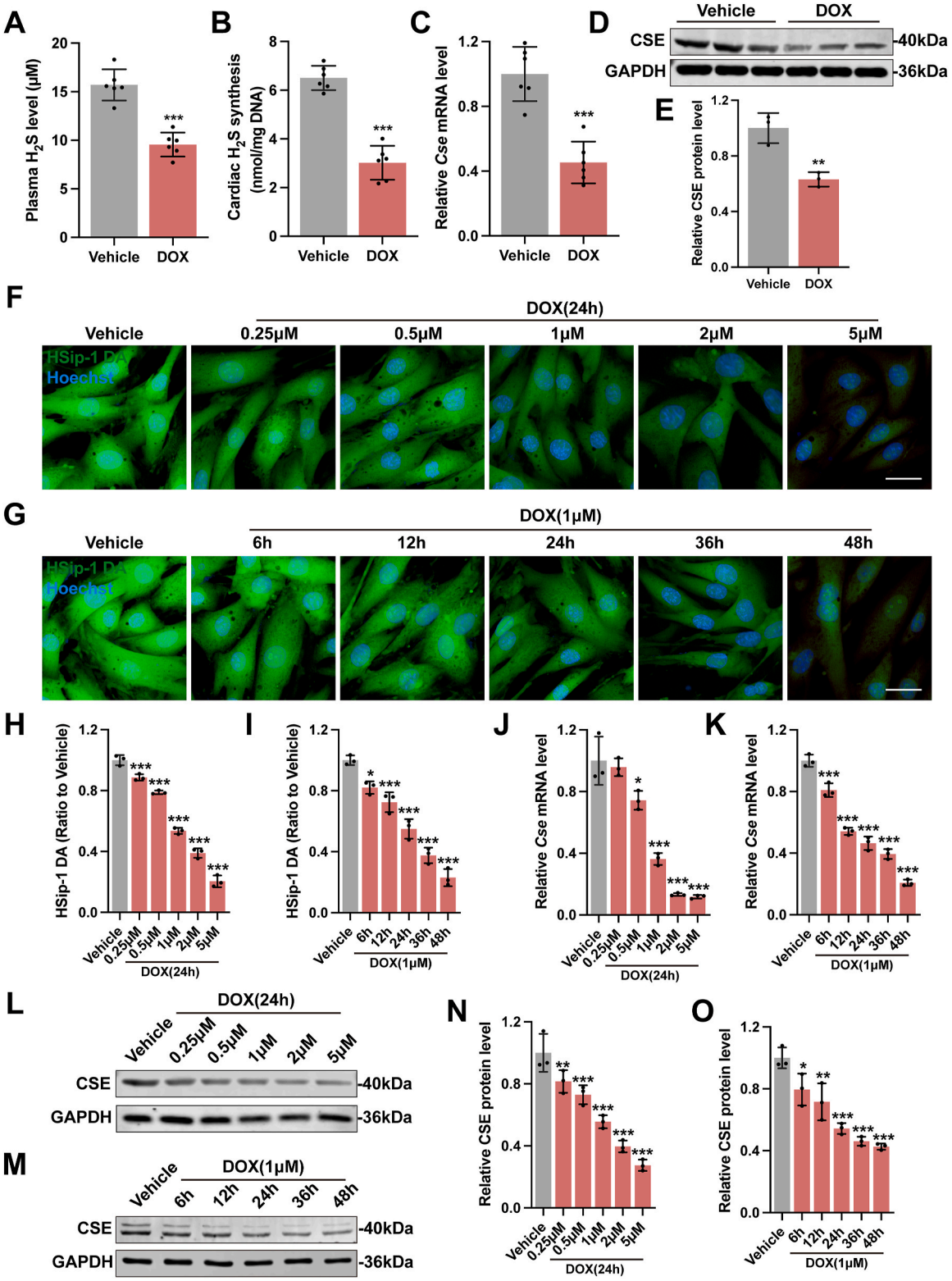

Fig. 1. Insufficient production of endogenous H_2S in cardiomyocytes in DoIC.
A, Plasma H_2S concentration in mice (n = 6). **B,** H_2S synthesizing activity in hearts (n = 6). **C,** The expression levels of *Cse* mRNA in heart tissues (n = 6). **D** and **E,** Representative blots and quantitative analysis of CSE protein levels in heart tissues (n = 3). **F** and **G,** Representative images of endogenous H_2S levels detected by the SulfoBiotics-HSip-1 DA fluorescent probe (Green) in H9c2 cells after a series of time gradient and concentration gradient doxorubicin stimulation (Scale bar indicated 20 μm), and the quantitative analysis of the fluorescence intensities were shown in **H** and **I** (n = 3). **J** and **K,** The expression levels of *Cse* mRNA in H9c2 cells after a series of time gradient and concentration gradient doxorubicin stimulation (n = 3). **L-O** Representative blots and quantitative analysis of CSE protein levels in H9c2 cells after a series of time gradient and concentration gradient doxorubicin stimulation (n = 3). The data are presented as the Mean ± SD. *p < 0.05, **p < 0.01 and ***p < 0.001 vs. Vehicle group. (For interpretation of the references to colour in this figure legend, the reader is referred to the Web version of this article.)

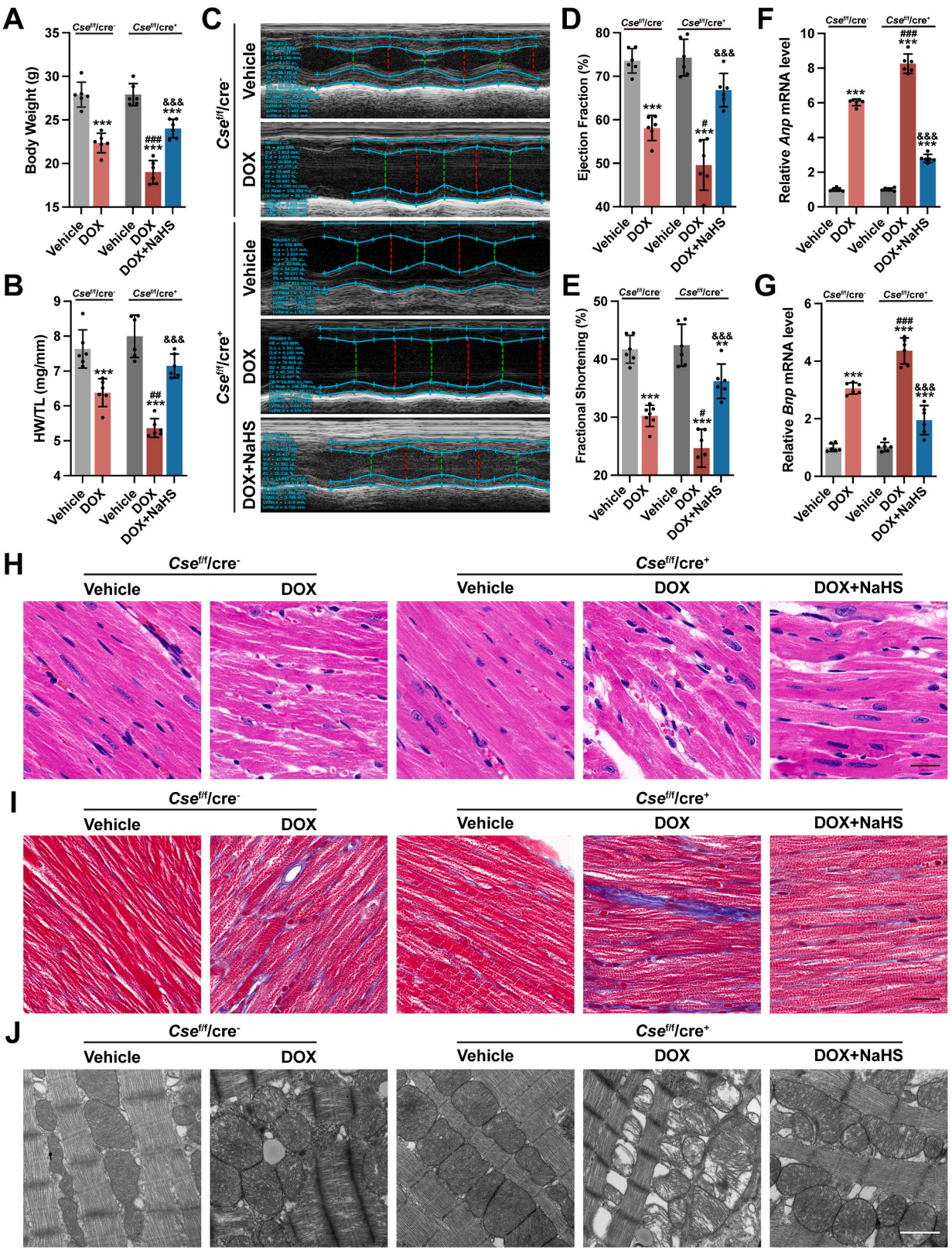

Fig. 2. Inhibition of endogenous H_2S production aggravated DoIC, which was partially rescued by exogenous H_2S supplementation.
A, Body weight of mice (n = 6). **B,** Ratio of heart weight to tibia length (HW/TL, n = 6). **C,** Representative M-mode images of transthoracic echocardiography. **D** and **E,** Quantification of left ventricular ejection fraction and left ventricular fraction shortening (n = 6). **F** and **G,** The expression levels of *Anp* and *Bnp* mRNA in heart tissues. **H,** Representative images of H&E staining in heart sections (Scale bar indicated 20 μm). **I,** Representative images of Masson's trichrome staining in heart sections (Scale bar indicated 20 μm). **J,** Representative transmission electron micrographs of heart tissues (Scale bar indicated 1 μm). The data are presented as the Mean ± SD. **p < 0.01 and ***p < 0.001 vs. Vehicle group at the same genetic background; #p < 0.05, ##p < 0.01 and ###p < 0.001 vs. DOX group of $Cse^{f/f}/cre^{-}$; &&&p < 0.001 vs. DOX group of $Cse^{f/f}/cre^{+}$.

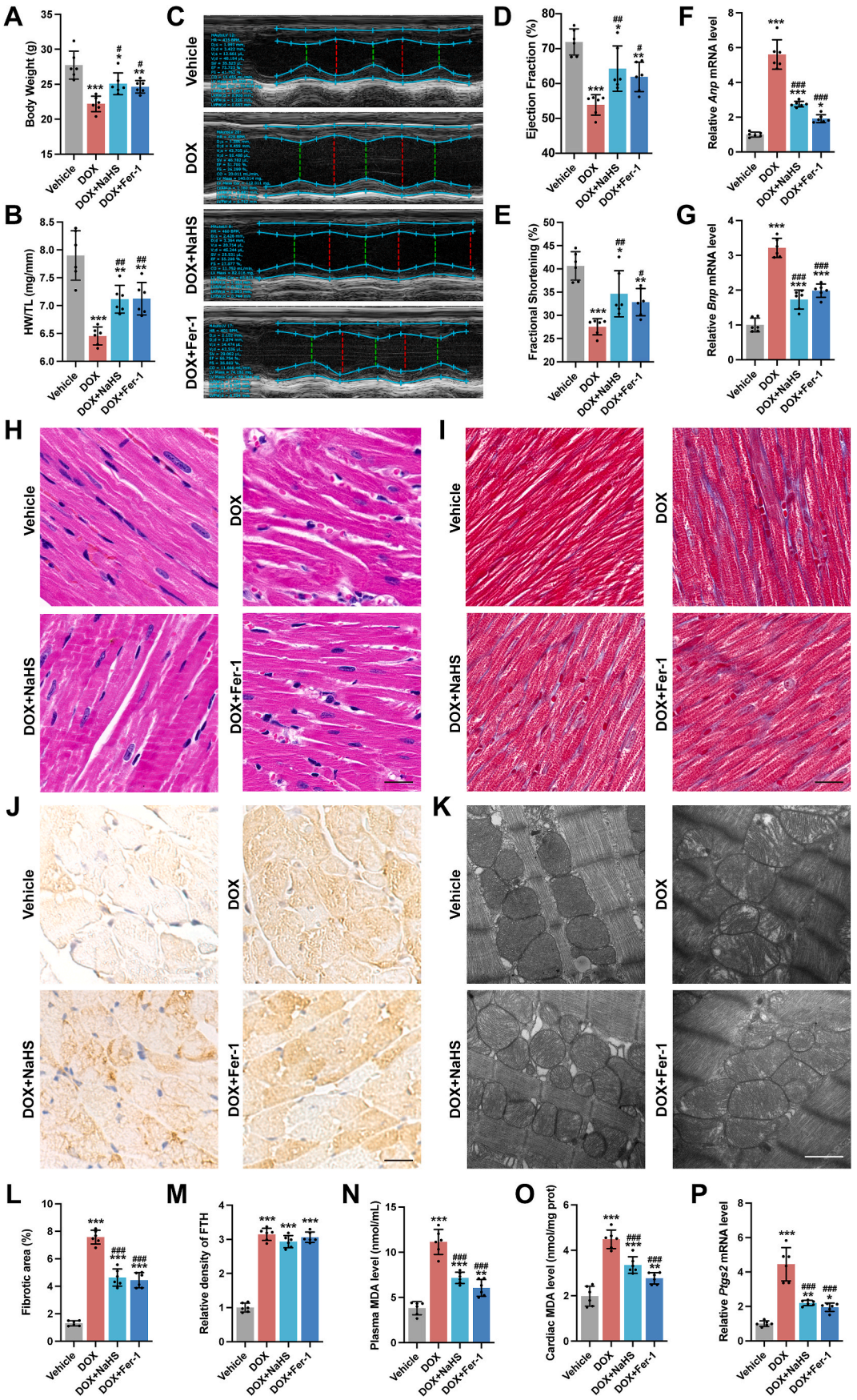

(caption on next page)

Fig. 3. H_2S ameliorated DoIC by inhibiting cardiomyocyte ferroptosis *in vivo*.
A, Body weight of mice (n = 6). **B,** Ratio of heart weight to tibia length (HW/TL, n = 6). **C,** Representative M-mode images of transthoracic echocardiography. **D** and **E,** Quantification of left ventricular ejection fraction and left ventricular fraction shortening (n = 6). **F** and **G,** The expression levels of *Anp* and *Bnp* mRNA in heart tissues (n = 6). **H,** Representative images of H&E staining in heart sections (Scale bar indicated 20 μm). **I,** Representative images of Masson's trichrome staining in heart sections (Scale bar indicated 20 μm), the percentage of fibrotic area was calculated in **L** (n = 6). **J,** Representative images of immunohistochemistry staining of FTH (Brown) in heart sections (Scale bar indicated 20 μm), the quantification analysis of FTH was shown in M (n = 6). **K**, Representative transmission electron micrographs of heart tissues (Scale bar indicated 1 μm). **N** and **O,** MDA levels in plasma and heart tissues (n = 6). **P,** The expression levels of *Ptgs2* mRNA in heart tissues (n = 6). The data are presented as the Mean ± SD. *p < 0.05, **p < 0.01 and ***p < 0.001 vs. Vehicle group; #p < 0.05, ##p < 0.01 and ###p < 0.001 vs. DOX group. (For interpretation of the references to colour in this figure legend, the reader is referred to the Web version of this article.)

phenylenediamine sulphate (20 μM) in 7.2 M HCl was added, followed by 40 μL $FeCl_3$ (30 μM) in 1.2 M HCl. Thereafter, 120 μL 10 % trichloroacetic acid was used to precipitate protein that might be present in the plasma. The resulting solution was centrifuged at 14,000 g for 5 min at 4 °C. The absorbance of the final solution was measured at 670 nm using a 96-well microplate reader (Bio-Tek, USA). The plasma concentration of H_2S was calculated against a calibration curve of NaHS.

2.6. H_2S synthesizing activity assay

H_2S synthesizing activity in heart homogenates was measured as previously described [31]. The reaction mixture containing 100 mM potassium phosphate buffer (pH 7.4), 20 mM L-cysteine, 2 mM pyridoxal 5′-phosphate and tissue homogenate was prepared in tightly sealed tubes on ice. Tubes were subsequently transferred to a water bath at 37 °C to initiate the reactions. After 30 min, 1 % zinc acetate was added to entrap synthesized H_2S and 10 % trichloroacetic acid was subsequently added to stop the reaction. Additionally, 20 μM N, N-dimethyl-p--phenylenediamine sulphate in 7.2 M HCl was added, followed by 30 μM $FeCl_3$ in 1.2 M HCl. The absorbance of the final solution was determined at 670 nm using spectrophotometry (Bio-Tek, USA). The concentration of H_2S in each reaction mixture was calculated against a calibration curve of NaHS. H_2S synthesizing activity in heart homogenates was expressed as nmol H_2S formed/mg DNA after being adjusted to the DNA concentration in heart homogenates.

2.7. Measurement of MDA content

Serum and cardiac malondialdehyde (MDA) levels were measured using a kit (Cat#A003, Nanjing Jiancheng, China) in accordance with the manufacturer's instructions.

2.8. Cell treatment and transfection

H9c2 rat cardiomyocytes were purchased from Type Culture Collection of the Chinese Academy of Sciences (Shanghai, China) and cultured in Dulbecco's modified Eagle's medium (DMEM) (Cat#11965092, Hyclone, USA) with 10 % fetal bovine serum (FBS) (Cat#10099141, Gibco, USA) and 1 % penicillin-streptomycin solution (P/S) (Cat#15070063, Gibco, USA) at 37 °C in a humidified incubator containing 95 % air and 5 % CO2. Cells were seeded on a 6-well plate or a 96-well plate before experiments and replaced with serum-free DMEM for 12 h when cells were cultured at about 80 % confluence. DOX treatment was implemented at different concentrations (0–5 μM) for 24 h or 1 μM for different times (0–48 h). To supplement exogenous H_2S, cells were incubated with NaHS (100 or 200 μM) during the DOX treatment. To suppress ferroptosis, cells were incubated with Fer-1 (2 μM) during the DOX treatment. To inhibit the activity of system xÇ⁻, cells were incubated with Erastin2 (a selective inhibitor of the system xÇ⁻, 2 μM; Cat#HY-139087, MedChemExpress, USA) during the DOX treatment. For *in vitro* knockdown of *Cse*, a small interfering RNA (siRNA) molecule (si*Cse*; Genomeditech, China) was synthesized. The target sequences were listed in Table S2. A random sequence molecule was synthesized as negative control. Cells were seeded at a density of 1 × 10^5 cells/mL in a well plate containing growth medium without antibiotics and incubated overnight. Lipofectamin™ 3000 (Cat#L3000015, Invitrogen, USA) was used according to the manufacturer's instruction for 48 h to transfect in OPTI-MEM reduced serum medium (Cat#31985088, Gibco, USA). The effects of these interventions were evaluated by real-time PCR and Western Blot. After complete intervention, cells or supernatants were collected for subsequent use.

2.9. Intracellular H_2S detection assay

Intracellular H_2S level was measured using the sensitive fluorescent probe SulfoBiotics-HSip-1 DA (Cat#SB22, DOJINDO, Japan) according to the manufacturer's protocols. Briefly, treated cells were washed and incubated in 5 μM HSip-1 DA working solution for 30 min at 37 °C. Hoechst 33342 staining solution for live cells (Cat#C1027, Beyotime Biotechnology, China) was used for counterstaining the nucleus. All images were obtained with Nikon Eclipse Ti fluorescence microscope (Nikon, Japan) and analyzed using Image J software.

2.10. Cell viability

Cells were seeded at a concentration of 5000 cells/well in a 96-well plate. Different treatments were implemented as described above. The cell viabilities of each group were detected using the enhanced Cell Counting Kit-8 (CCK-8; Cat#C0042, Beyotime Biotechnology, China) for measuring the absorbance values at a wavelength of 450 nm 2 h after adding the working solution.

2.11. Flow cytometry-based lipid peroxidation assay

Cells were seeded in a 6-well plate and treated as indicated. After treatment, the cells were incubated in 2 μM BODIPY™ 581/591C11 regent (Cat#D3861, Invitrogen, USA) for 30 min at 37 °C in the dark, then analyzed using a CytoFLEXS flow cytometer (Beckman, USA). Data were collected from a minimum of 10,000 cells per sample and analyzed in the FlowJo 10.0 software.

2.12. Reactive oxygen species (ROS) generation

The H9c2 cells were cultured in 6-well plates and treated as above. ROS in cells was monitored using a Fluorometric Intracellular ROS Kit (Cat#MAK142; Sigma, USA) according to the manufacturer's instructions. Hoechst 33342 staining solution for live cells was used for counterstaining the nucleus. The level of intracellular ROS was detected with Nikon Eclipse Ti fluorescence microscope (Nikon, Japan) and analyzed using Image J software.

2.13. Analysis of mitochondrial membrane potential

Mitochondrial membrane potential was measured using the sensitive fluorescent probe JC-1 (Cat#T3168, Invitrogen, USA) according to the manufacturer's protocols. Briefly, treated cells were washed and incubated in 1 μM JC-1 working solution for 30 min at 37 °C. Hoechst 33342 staining solution for live cells was used for counterstaining the nucleus. All images were obtained with Nikon Eclipse Ti fluorescence microscope (Nikon, Japan) and analyzed using Image J software. Results were shown as a ratio of fluorescence measured at 485 nm/535 nm to that

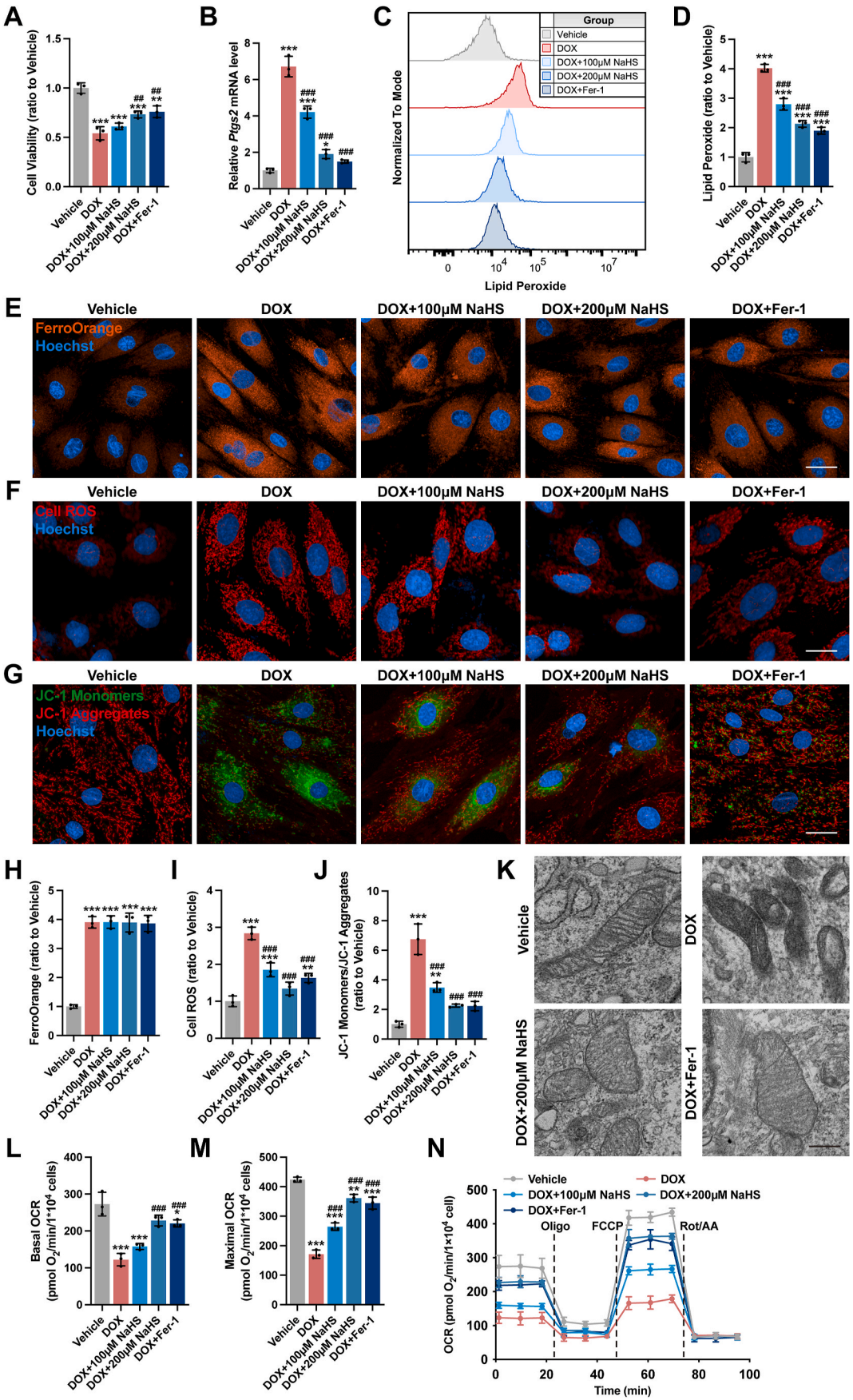

(caption on next page)

Fig. 4. H_2S ameliorated DoIC by inhibiting cardiomyocyte ferroptosis *in vitro*.
A, Cell viability of H9c2 cells (n = 3). **B,** The expression levels of *Ptgs2* mRNA in H9c2 cells (n = 3). **C** and **D,** Representative images and quantification of intracellular lipid peroxide in H9c2 cells (n = 3). **E,** Representative images of intracellular Fe^{2+} level detected by FerroOrange staining (Orange) in H9c2 cells, and the quantitative analysis of the fluorescence intensities were shown in **H** (n = 3). **F,** Representative images of intracellular ROS level detected by cell ROS fluorescent probe (Red) in H9c2 cells, and the quantitative analysis of the fluorescence intensities were shown in **I** (n = 3). **G,** Representative images of mitochondrial membrane potential detected by JC-1 fluorescent probe in H9c2 cells, and the quantitative analysis was established as the ratio of the JC-1 Monomers (Green) and JC-1 Aggregates (Red) in **J** (n = 3). **K,** Representative transmission electron micrographs of H9c2 cells (Scale bar indicated 1 μm). **L-N,** Real-time oxygen consumption rates (OCR) and calculated basal and maximal respiration rates in H9c2 cells (n = 3). The data are presented as the Mean ± SD. *p < 0.05, **p < 0.01 and ***p < 0.001 vs. Vehicle group; ##p < 0.01 and ###p < 0.001 vs. DOX group. (For interpretation of the references to colour in this figure legend, the reader is referred to the Web version of this article.)

measured at 535 nm/590 nm (monomers to aggregates fluorescence).

2.14. Oxygen consumption measurements

Measurement of oxygen consumption rate of H9c2 cells was performed using seahorse XF Cell Mito Stress Test Kit (Cat#103010, Agilent, USA) performed by Seahorse XF96e Extracellular Flux Analyzer (Agilent, USA). 1×10^4 H9c2 cells were seeded on Seahorse cell culture plates and treated according to aforementioned protocol. The completed culture media were changed to Seahorse XF DMEM supplemented with 5 μM glucose, 1 μM pyruvate and 10 μM glutamine. After 1 h incubation at 37 °C in CO2-free incubator, oxygen consumption was measured following respective injections with a blank, oligomycin (1.5 M), FCCP (1 M), and Rotenone/Antimycin A (0.5 M). Oxygen consumption measurements were normalized to total cell number determined by DAPI stained nucleus counting at the end of the experiment.

2.15. Glutathione level assay

Heart homogenates or cell lysates were collected for GSH analysis using a total GSH/oxidized GSH assay kit (Cat#A061, Nanjing Jiancheng, China) in triplicate according to the manufacturer's instructions. The results were normalized to total protein concentration tested by the bicinchoninic acid method.

2.16. Supernatant glutamate level assay

The release of glutamate from H9c2 cells into the extracellular medium was detected using a WST based glutamate assay kit (Cat#G269, DOJINDO, Japan). The H9c2 cells were seeded in 6-well plates and treated as above. The supernatants of each well were collected and tested in triplicate according to the manufacturer's instructions. Supernatant glutamate level was normalized to total cell number determined by DAPI stained nuclei counting at the end of the experiment.

2.17. Quantitative real-time PCR

Total RNA was isolated from cardiac tissues or cells using TRIzol regent (Cat#15596018, Invitrogen, USA), and RNA concentration and purity were measured using Nanodrop 3100 (Thermo Scientific, USA). RNA was reverse-transcribed using HiScriptII Reverse Transcriptase kit (Cat#R201, Vazyme, China) in accordance with the manufacturer's instructions, and quantitative PCR was conducted in triplicate using an Applied Biosystems 6Flex with SYBR Green Master Mix (Cat#B21703, Bimake, USA). The fold difference in gene expression was calculated using the $2^{-\triangle\triangle Ct}$ method and was presented relative to *Gapdh* mRNA. The sequences of the forward and reverse primers used for amplification were shown in Table S3.

2.18. Western immunoblot

To obtain total protein extracts, cultured cells or frozen cardiac tissues were lysed at 4 °C in radioimmunoprecipitation (RIPA) buffer with protease and phosphatase inhibitor cocktail (Cat#P1050, Beyotime Biotechnology, China). Tissue homogenates or cell lysates were clarified by centrifugation at 14,000 g for 15 min at 4 °C and the protein concentration was determined using the bicinchoninic acid method (Cat#P0010S, Beyotime Biotechnology, China). A total of 20 μg protein per sample was size-fractionated by sodium dodecyl sulphate polyacrylamide gel electrophoresis and transferred onto Immobilon polyvinylidene difluoride membranes (Millipore, USA). The membranes were blocked for 2 h with 5 % DifcoTM Skim Milk (Cat#232100, BD Biosciences, USA) and then probed overnight at 4 °C with primary antibodies (Table S1), followed by a 1:30,000 dilution of Dylight™ 800 4XPEG-conjugated goat anti-rabbit IgG (H + L) or goat anti-mouse IgG (H + L) (Cell Signaling Technology, USA) for an hour. The results were visualized and analyzed by Odyssey Infrared Imaging System.

2.19. Co-immunoprecipitation (Co-IP)

H9c2 cells were harvested and lysed as previously described. Cell lysates were incubated with anti-Keap1 antibody (1 μg/mg protein; Table S1) or normal rabbit IgG overnight at 4 °C, followed by incubating with 30 μL BSA blocked Protein A/G magnetic beads (Cat# B23201, Bimake, USA) for 6 h at 4 °C. The precipitated beads were washed 3 times with ice-cold immunoprecipitation lysis buffer and proteins were eluted in SDS loading buffer (Cat# P0015B, Beyotime Biotechnology, China) by incubating at 95 °C for 10 min. The eluted proteins were analyzed by immunoblotting.

2.20. Immunofluorescence staining

H9c2 cells were rinsed with PBS, fixed with 4 % paraformaldehyde for 20 min at room temperature, blocked by incubation with PBS containing 10 % goat serum (Cat#C0265, Beyotime Biotechnology, China) and 0.3 % Triton-100 (Cat#9036-19-5, Sigma-Aldrich, USA) for 1 h at 37 °C and incubated with primary antibodies (Table S1) overnight at 4 °C. After additional washing, cells were incubated with Alexa Fluro conjugated secondary antibody (Table S1) for 1 h at room temperature. Nuclei were stained using 4′,6-diamidino-2-phenylindole (DAPI) for 10 min. Image acquisition was performed using Nikon Eclipse Ti fluorescence microscope (Nikon, Japan) and analyzed using Image J software.

2.21. Biotin switch assay of S-sulfhydration

A biotin switch assay was performed utilizing a biotin switch assay kit (Cat#ab236207, Abcam, USA) with little modifications [28,29]. Briefly, treated H9c2 cells were homogenized in HEN buffer (250 mM HEPES-NaOH [pH 7.7] supplemented with 1 mM EDTA and 0.1 mM neocuproine) containing 150 μM deferoxamine, 1 % Nonidet-P40 (NP-40), and protease/phosphatase inhibitors. The lysates were added to HEN buffer supplemented with 2.5 % SDS and 20 mM methyl methanethiosulfonate (MMTS). The samples were frequently shaken at 50 °C for 30 min. Then, the MMTS was removed by adding acetone and the samples were precipitated at −20 °C for 1 h. The pellets were suspended in HEN buffer containing 1 % SDS and 4 mM biotin-HPDP. After 3 h of incubation at 25 °C, the proteins were purified with acetone. Finally, the proteins were dissolved in solution buffer, purified with streptavidin–agarose beads and subjected to western blotting with an anti-Keap1 antibody (Table S1). Cells treated by dithiothreitol (DTT) (1

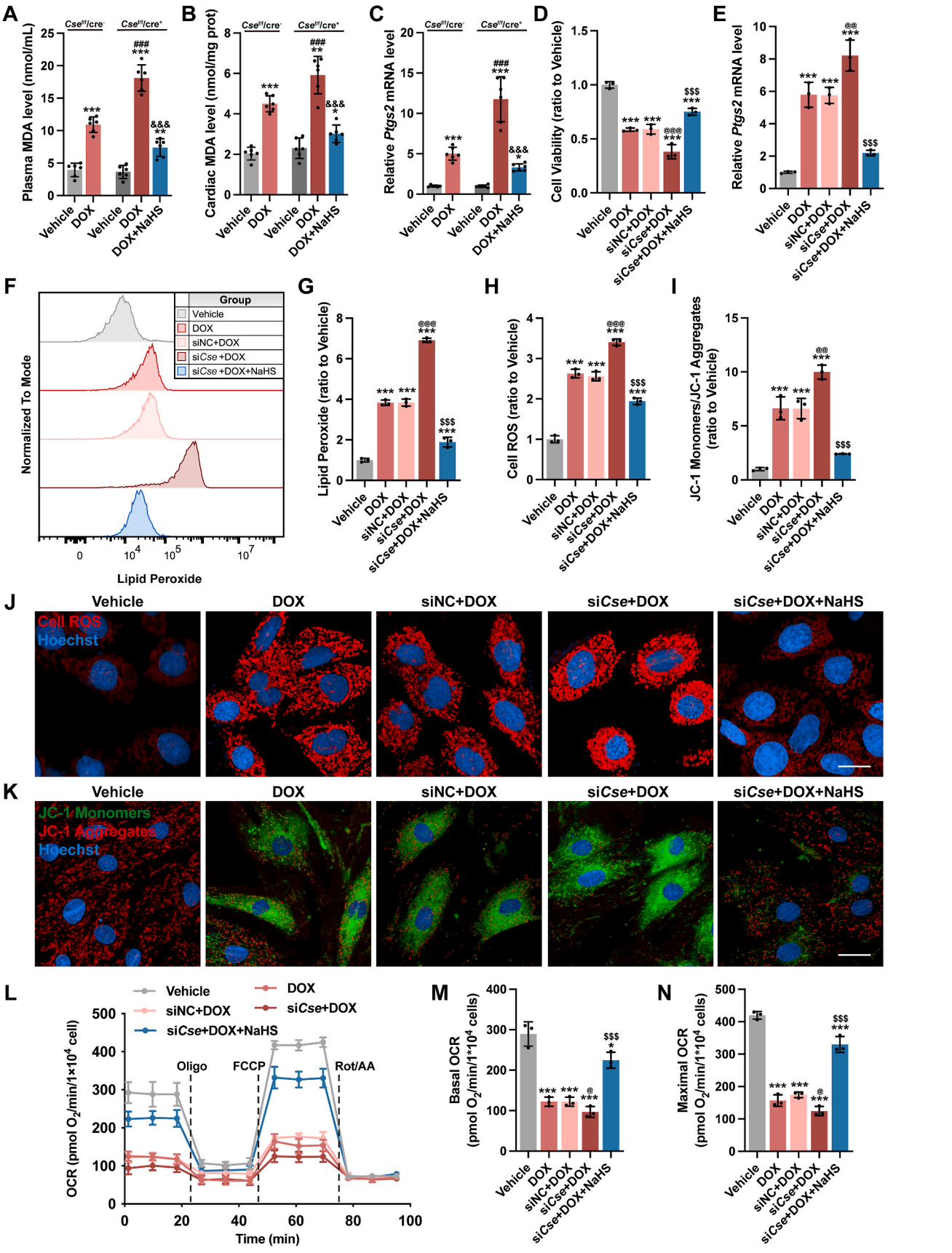

(caption on next page)

Fig. 5. Cardiac knockout of *Cse* gene in mice or knockdown *Cse* gene in H9c2 cells aggravated DOX-induced ferroptosis.
A and **B,** MDA level in plasma and heart tissues (n = 6). **C,** The expression levels of *Ptgs2* mRNA in heart tissues (n = 6). **D,** Cell viability of H9c2 cells (n = 3). **E,** The expression levels of *Ptgs2* mRNA in H9c2 cells (n = 6). **F** and **G,** Representative images and quantification of intracellular lipid peroxide in H9c2 cells (n = 3). **J,** Representative images of intracellular ROS level detected by cell ROS fluorescent probe (Red) in H9c2 cells, and the quantitative analysis of the fluorescence intensities were shown in **H** (n = 3). **K,** Representative images of mitochondrial membrane potential detected by JC-1 fluorescent probe in H9c2 cells, and the quantitative analysis was established as the ratio of the JC-1 Monomers (Green) and JC-1 Aggregates (Red) in **I** (n = 3). **L-N,** Real-time oxygen consumption rates (OCR) and calculated basal and maximal respiration rates in H9c2 cells (n = 3). The data are presented as the Mean ± SD. For panel **A-C**, *p < 0.05, **p < 0.01 and ***p < 0.001 vs. Vehicle group at the same genetic background; ###p < 0.001 vs. DOX group of $Cse^{f/f}$/cre^{-}; &&&p < 0.001 vs. DOX group of $Cse^{f/f}$/cre^{+}. For panel **D-N**, *p < 0.05 and ***p < 0.001 vs. Vehicle group; @p < 0.05, @@p < 0.01 and @@@p < 0.001 vs. siNC + DOX group; $$$p < 0.001 vs. si*Cse* + DOX group. (For interpretation of the references to colour in this figure legend, the reader is referred to the Web version of this article.)

mmol/L) served as the negative control group.

2.22. Transmission electron microscopy (TEM)

For TEM morphological analysis, freshly excised heart tissues or cell pellets were fixed in 2.5 % glutaraldehyde in 0.1 M sodium cacodylate buffer (pH 7.4) at 4 °C for 2 h. After being washed with 0.1 M sodium cacodylate buffer, they were post-fixed with 1 % osmium tetroxide for 2 h and dehydrated through a graded ethanol series at 4 °C. Finally, the samples were embedded in epoxy resin at room temperature for 4 h. Ultrathin sections (70 nm) were assembled to a copper grid and observed using electron microscopy (Hitachi, Japan).

2.23. Statistical analysis

All arithmetic data were expressed as the mean ± SD at least 6 mice *in vivo* and 3 independent experiments *in vitro*. A two-tailed Student's t-test was used to compare means between two groups and one-way ANOVA followed by Tukey's multiple comparison was used to analyze the differences among more than 3 groups. Statistical analysis was performed using GraphPad Prism 9.0. A p-value <0.05 was considered statistically significant.

3. Results

3.1. Disturbance of endogenous H_2S metabolism in hearts in DoIC

A classic mouse model of chronic DoIC was applied to explore the changes of endogenous H_2S metabolism in cardiomyocytes. As shown in Fig. 1A and B, the plasma level of H_2S and cardiac H_2S synthesizing activity in DOX group markedly reduced as compared with vehicle group. Meanwhile, the cardiac mRNA and protein expression of CSE, a crucial H_2S generating enzyme in cardiovascular system, was significantly downregulated by DOX (Fig. 1C–E). Additionally, we evaluated the mRNA and protein expression of MPST and CBS, two other major H_2S production enzymes. The cardiac expression of MPST did not significantly alter during the induction of DoIC while CBS was minimally expressed in heart tissues (Figs. S2A–S2C).

On the other hand, H9c2 rat cardiomyocytes were incubated with DOX at gradient concentrations ranging from 0.25 to 5.0 μM or for different time periods. Intracellular H_2S level was detected by SulfoBiotics-HSip-1 DA, a sensitive fluorescent probe verified by the gradient NaHS intervention test (Figs. S2D and S2E). Not surprisingly, DOX decreased the intracellular H_2S level in H9c2 cells in a dose-dependent and time-dependent manner (Fig. 1F–I). Coincidently, the mRNA and protein expression of CSE was also dose-dependently and time-dependently downregulated by DOX (Fig. 1J–O). Taken together, these findings suggested that DOX suppressed the expression of CSE in cardiomyocytes and caused endogenous H_2S insufficiency in DoIC.

3.2. Mice with cardiac loss of CSE ($Cse^{f/f}$/Cre^{+}) developed more severe DoIC

To verify the role of H_2S in DoIC, cardiomyocyte-specific *Cse* knockout mice ($Cse^{f/f}$/Cre^{+}) were generated using LoxP-targeting system. Since a recent research showed that cardiomyocyte-specific Cre recombinase expression caused a dilated cardiomyopathy with ferroptosis-like phenotype in 6-month-old mice [32], we first verified that the 8-week-old, Cre-ERT2 mice we used showed no difference in cardiac function (Figs. S3A–S3G), histology (Fig. S3H), and ferroptotic phenotypes (Fig. S3I-S3N) compared to wild-type mice of the same age. Then, cardiac Cse deletion was induced by Tamoxifen right before start of induction of DoIC (Fig. S1B), the genotype identification was shown in Fig. S4A. The cardiac CSE protein level was significantly suppressed by Tamoxifen induction in $Cse^{f/f}$/Cre^{+} mice (Figs. S4B and S4C), followed by the decreased H_2S levels both in plasma (Fig. S4D) and cardiac tissues (Fig. S4E).

As shown in Fig. 2A–G, DOX caused myocardial injury and heart failure, as characterized by an obvious reduction in body weight (BW) and the ratio of heart weight to tibia length (HW/TL), ejection fraction (EF) and fraction shortening (FS) evaluated by echocardiography, and an apparent rise in *Anp* and *Bnp* mRNA levels, two classic biomarkers of heart failure. Histologically, cardiac tissue was seriously damaged in DOX group, as indicated by ruptured cardiomyocytes and disordered myocardial fibers, with a certain degree of inter-myocardial fibrosis. Cardiac depletion of endogenous H_2S production in $Cse^{f/f}$/Cre^{+} mice significantly aggravated DoIC. A further decline in BW, HW/TL, EF and FS, along with an extra rise in *Anp* and *Bnp* mRNA level (Fig. 2A–G) was observed in $Cse^{f/f}$/Cre^{+} mice injected with DOX. Impairment in the histology of cardiac muscles was also augmented by cardiomyocyte-specific deletion of *Cse* (Fig. 2H and I). Consistent with developing more severe DoIC, $Cse^{f/f}$/Cre^{+} mice displayed exacerbated mitochondrial damage, as characterized by more obvious mitochondrial swelling and vacuolization with disintegration and lysis of cristae in cardiomyocytes (Fig. 2J). All the deteriorations observed in DOX-injected $Cse^{f/f}$/Cre^{+} mice were substantially reversed by a long-term low-dose supplementation of exogenous H_2S (Fig. 2A–J). Altogether, these results proposed a protective role of endogenous H_2S in the process of chronic DoIC.

3.3. H_2S ameliorated DoIC by inhibiting ferroptosis in cardiomyocytes

Recent studies have revealed that ferroptosis, a newly defined iron-dependent cell death, plays a key role in DoIC [9]. Then, we investigated the potential effect of H_2S on ferroptosis in DoIC. During the induction of DoIC, mice received daily intraperitoneal injections of NaHS or Fer-1, a ferroptosis inhibitor by eliminating lipid peroxides. Both NaHS and Fer-1 ameliorated the loss of BW and HW/TL, cardiac dysfunction and the increase in cardiac *Anp* and *Bnp* mRNA level caused by DOX (Fig. 3A–G). Besides, both NaHS and Fer-1 alleviated DOX-induced morphological alterations and myocardial fibrosis in heart tissues (Fig. 3H, I and 3L). Further, as same as Fer-1, H_2S significantly reduced lipid peroxide production, including decreased serum and cardiac MDA levels (Fig. 3N and O) and downregulated *Ptgs2* mRNA expression, a classic marker of ferroptosis (Fig. 3P), thereby partially restoring mitochondrial ultrastructure in cardiomyocytes (Fig. 3K). However, both Fer-1 and H_2S had no effect on DOX-induced iron accumulation in cardiomyocytes (Fig. 3J and M).

To ascertain the relationship between H_2S and ferroptosis in DoIC, H9c2 cells were pretreated with NaHS or Fer-1 before incubation with

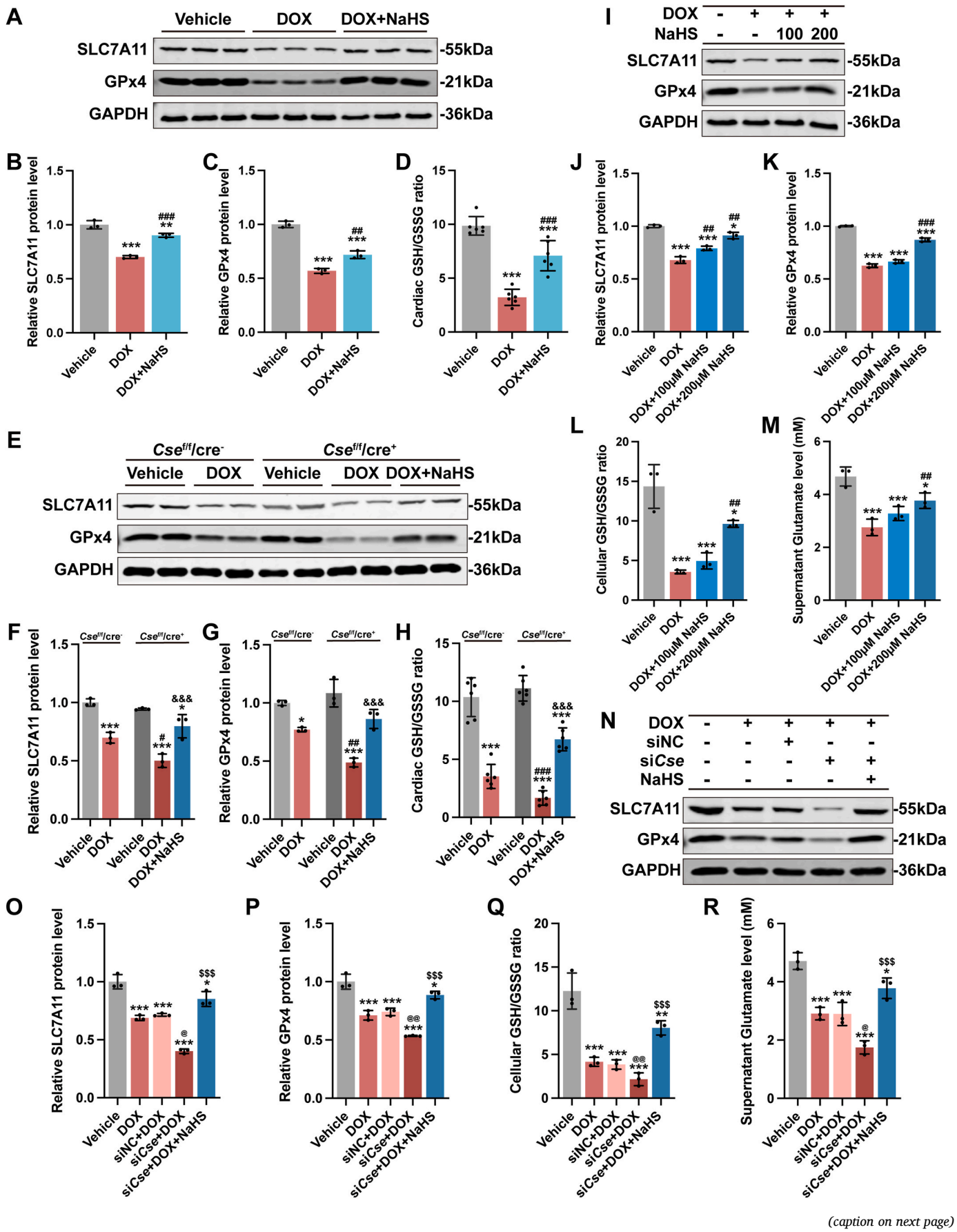

(caption on next page)

Fig. 6. H_2S inhibited DOX-induced cardiomyocyte ferroptosis via regulating SLC7A11/GSH/GPx4 pathway.
A-C, Representative blots and quantitative analysis of SLC7A11 and GPx4 protein levels in heart tissues (n = 3). **D,** the ratio of the GSH and GSSG in heart tissues (n = 6). **E-G,** Representative blots and quantitative analysis of SLC7A11 and GPx4 protein levels in heart tissues (n = 3). **H,** the ratio of the GSH and GSSG in heart tissues (n = 6). **I–K,** Representative blots and quantitative analysis of SLC7A11 and GPx4 protein levels in H9c2 cells (n = 3). **L,** the ratio of the GSH and GSSG in H9c2 cells (n = 3). **M,** The glutamate levels of supernatants from cultured H9c2 cells (n = 3). **N–P,** Representative blots and quantitative analysis of SLC7A11 and GPx4 protein levels in H9c2 cells (n = 3). **Q,** the ratio of the GSH and GSSG in H9c2 cells (n = 3). **R,** The glutamate levels of supernatants from cultured H9c2 cells (n = 3). The data are presented as the Mean ± SD. For panel **F–H**, *p < 0.05 and ***p < 0.001 vs. Vehicle group at the same genetic background; #p < 0.05, ##p < 0.01 and ###p < 0.001 vs. DOX group of $Cse^{f/f}$/cre$^-$; &&&p < 0.001 vs. DOX group of $Cse^{f/f}$/cre$^+$. For the rest of panels, *p < 0.05, **p < 0.01 and ***p < 0.001 vs. Vehicle group; ##p < 0.01 and ###p < 0.001 vs. DOX group; @p < 0.05 and @@p < 0.01 vs. siNC + DOX group; $$$p < 0.001 vs. si*Cse* + DOX group.

DOX. NaHS dose-dependently reversed DOX-induced suppression of cell viability, which could be mimicked by pretreatment with Fer-1 (Fig. 4A). Besides, similar to Fer-1, NaHS significantly inhibited DOX-induced ferroptosis, as evidenced by a dose-dependent reduction in *Ptgs2* mRNA expression (Fig. 4B) and lipid peroxide level (Fig. 4C and D). Further, in coincidence with the findings *in vivo*, both NaHS and Fer-1 markedly suppressed ROS production (Fig. 4F and I) and restored mitochondrial dysfunction and ultrastructure damage as characterized by an obvious increase in mitochondrial membrane potential (Fig. 4G and J), improved mitochondrial respiration capacity (Fig. 4L–N) as well as less swollen mitochondria with cristae loss (Fig. 4K). However, neither NaHS nor Fer-1 restrained iron accumulation in DOX-stimulated H9c2 cells (Fig. 4E and H). Taken together, both *in vivo* and *in vitro* findings suggested that H_2S attenuated DOX-induced cardiomyocyte ferroptosis by inhibiting accumulation of lipid peroxide.

3.4. Cardiac loss of Cse aggravated DOX-induced ferroptosis in cardiomyocytes

Cse cardiac-specific knockout mice were used to further validate our findings about H_2S and DOX-induced ferroptosis. In contrast to DOX-injected $Cse^{f/f}$/Cre$^-$ mice, plasma and cardiac MDA levels (Fig. 5A and B) and *Ptgs2* mRNA expression (Fig. 5C) significantly elevated in DOX-injected $Cse^{f/f}$/Cre$^+$ mice. The aggravation of MDA production and ferroptosis in DOX-injected $Cse^{f/f}$/Cre $^+$ mice was abrogated by supplementation of exogenous H_2S.

On the other hand, siRNA for *Cse* (si*Cse*) was constructed and transfected into H9c2 cells. The transfection efficiency was shown in Figs. S5A–S5C, and the cellular H_2S level was significantly decreased in the *Cse* knockdown cells (Figs. S5D and S5E). Under stimulation of DOX, H9c2 cells with si*Cse* transfection showed lower cell viability (Fig. 5D), higher *Ptgs2* mRNA expression (Fig. 5E) and more lipid peroxide accumulation (Fig. 5F and G). Besides, si*Cse* transfection further increased the intracellular level of ROS (Fig. 5H and J) and exacerbated mitochondrial impairment, as characterized by an obvious decline in mitochondrial membrane potential (Fig. 5I and K) and mitochondrial respiration capacity (Fig. 5L–N). All these changes could be partially reversed by supplementation with exogenous H_2S. Collectively, both *in vivo* and *in vitro* findings suggested that H_2S attenuated DOX-induced cardiomyocyte ferroptosis by inhibiting accumulation of lipid peroxide.

3.5. H_2S inhibited DOX-induced ferroptosis by SLC7A11/GSH/GPx4 pathway

SLC7A11/GSH/GPx4 signaling axis is the canonical ferroptosis defense pathway [10]. SLC7A11, a cystine/glutamate antiporter (also commonly known as xCT) mediates the uptake of extracellular cystine in exchange for glutamate [27]. Cystine is converted to cysteine to synthesize GSH. GPx4 then uses GSH as a co-factor to reduce lipid peroxides and prevent ferroptosis [27]. Therefore, we investigated the association between H_2S and SLC7A11/GSH/GPx4 pathway in DOX-induced ferroptosis.

In the murine model of DoIC, DOX significantly downregulated the expression of SLC7A11 (Fig. 6A and B) and GPx4 (Fig. 6A and C) in hearts and consequently decreased the GSH/GSSG ratio (Figs. S6A and S6B and Fig. 6D). Administration of NaHS remarkably mitigated DOX-induced downregulation of SLC7A11, GPx4 and the GSH/GSSG ratio in hearts (Fig. 6A–D, Figs. S6A and S6B). In sharp contrast, cardiac knockout of *Cse* in mice with DOX injection exacerbated the reduction in expression of SLC7A11 (Fig. 6E and F) and GPx4 (Fig. 6E and G), and the GSH/GSSG ratio (Fig.S6C, S6D and Fig. 6H). The exacerbation was partially rescued by exogenous H_2S supplementation (Fig. 6E–H, Figs. S6C and S6D).

In H9c2 cells, DOX downregulated the expression of SLC7A11 (Fig. 6I and J) and GPx4 (Fig. 6I and K) and decreased the GSH/GSSG ratio (Figs. S6E and S6F and Fig. 6L) and glutamate level (Fig. 6M). NaHS dose-dependently attenuated the alterations in SLC7A11/GSH/GPx4 pathway caused by DOX (Fig. 6I–M, Figs. S6E and S6F). However, transfection with si*Cse* aggravated them (Fig. 6N–R, Figs. S6G and S6H), which was partially abrogated by addition of NaHS.

Erastin2 is a potent inhibitor of the system xÇ$^-$ cystine/glutamate transporter and triggers ferroptosis in many cell types [33,34]. In accordance with the literature, Erastin2 not only inhibited the expression of SLC7A11 and GPx4 in H9c2 cells but also aggravated the inhibitory effect in DOX-stimulated H9c2 cells (Figs. S7A–7C). As a result, Erastin2 caused more severe lipid peroxidative damage and mitochondrial dysfunction in DOX-stimulated H9c2 cells in comparison to unstimulated cells (Figs. S7D–7F). Notably, pretreatment with NaHS had negligible effect on the expression of SLC7A11 and GPx4 as well as the process of ferroptosis (Fig. S7).

Pretreatment with Erastin2 in DOX-stimulated H9c2 cells significantly abrogated the upregulation of SLC7A11 (Fig. 7A and B) and GPx4 expression (Fig. 7A and C) caused by NaHS. As a result, NaHS could not restore DOX-induced ferroptosis in the presence of Erastin2. In DOX + NaHS + Erastin2 group, GSH/GSSG ratio (Figs. S6I and S6J and Fig. 7D), supernatant glutamate level (Fig. 7E) and cell viability (Fig. 7F) were apparently lower than those in DOX + NaHS group whereas *Ptgs2* expression (Fig. 7G), lipid peroxides (Fig. 7H and I) and intracellular ROS (Fig. 7J and K) were much higher. An obvious impairment in mitochondrial membrane potential (Fig. 7L and M) and mitochondrial respiration capacity (Fig. 7N–P) was also observed in the DOX + NaHS + Erastin2 group. Collectively, these observations indicated that inhibition of system xÇ$^-$ abolished the protective effect of NaHS in DOX-induced cardiomyocyte ferroptosis, suggesting the involvement of SLC7A11/GSH/GPx4 pathway in the anti-ferroptosis activity of H_2S.

3.6. H_2S promoted SLC7A11 and GPx4 transcription by inducing Keap1 S-sulfhydration and Nrf2 activation

To determine the potential mechanism of H_2S in regulating SLC7A11/GSH/GPx4 pathway, we examined the Keap1-Nrf2 signaling axis, which regulates oxidative stress-induced SLC7A11 and GPx4 transcription [27]. Interestingly, DOX treated significantly upregulated the expression of Keap1 (Fig. 8A and D) and increased the Nrf2/Keap1 interaction (Fig. 8A–C), which led to a decreased protein level (Fig. 8A and E) and an inhibition of nuclear translocation of Nrf2 (Fig. 8F and G), thus decreased the transcription of SLC7A11 and GPx4 (Fig. 8H). Administration of NaHS, although had no effect in the expression of Keap1, partially increased Nrf2 dissociation from Keap1 and reversed the protein level and nuclear translocation of Nrf2, promoting SLC7A11 and GPx4 transcription (Fig. 8A–H). S-sulfhydration, the addition of one sulfhydryl to the thiol side of the cysteine residue and formation of a

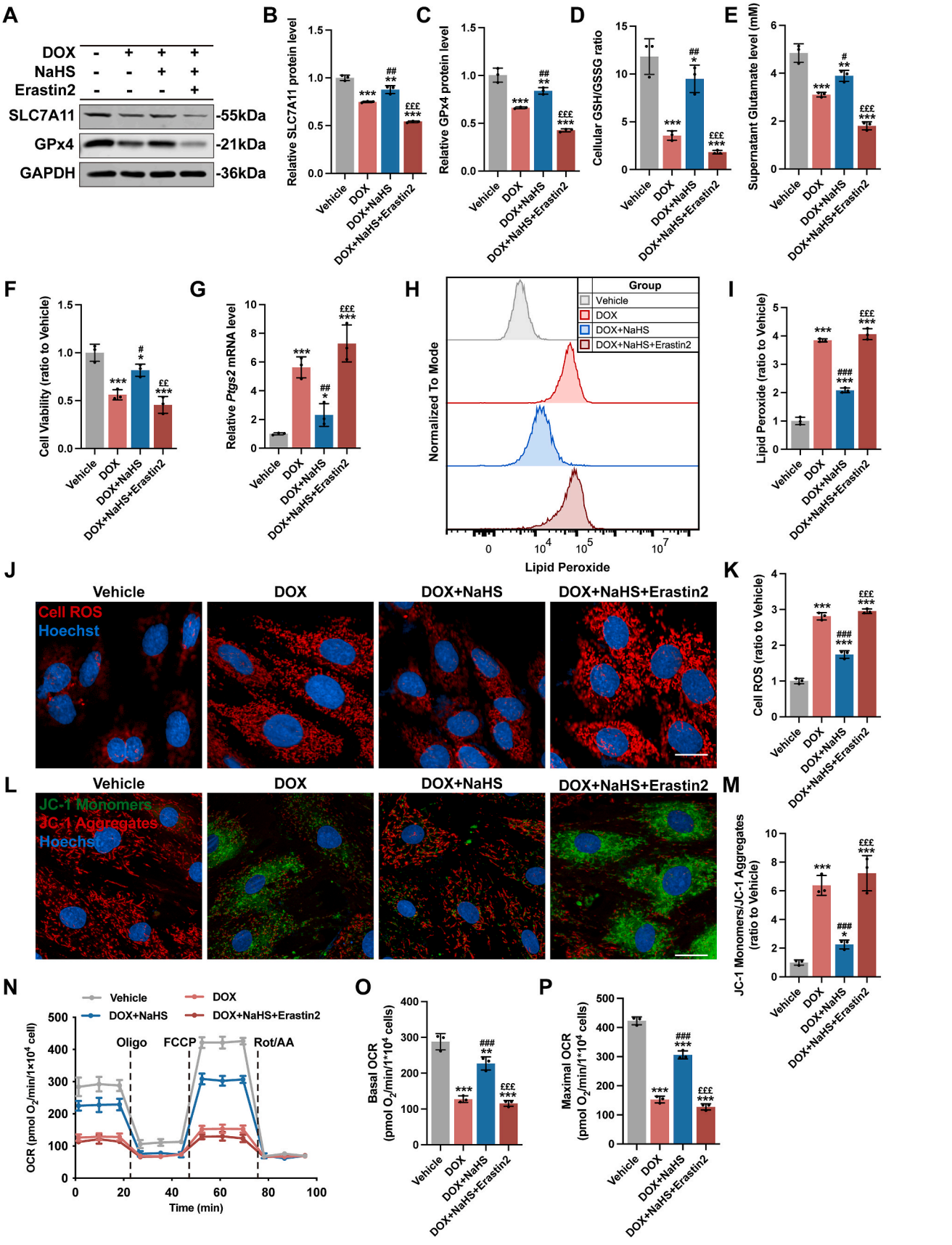

(caption on next page)

Fig. 7. Inhibition of SLC7A11 counteracted the protective effect of H_2S on DOX-induced cardiomyocyte ferroptosis.
A-C, Representative blots and quantitative analysis of SLC7A11 and GPx4 protein levels in H9c2 cells (n = 3). **D,** the ratio of the GSH and GSSG in H9c2 cells (n = 3). **E,** The glutamate levels of supernatants from cultured H9c2 cells (n = 3). **F,** Cell viability of H9c2 cells (n = 3). **G,** The expression levels of *Ptgs2* mRNA in H9c2 cells (n = 3). **H** and **I,** Representative images and quantification of intracellular lipid peroxide in H9c2 cells (n = 3). **J,** Representative images of intracellular ROS level detected by cell ROS fluorescent probe (Red) in H9c2 cells, and the quantitative analysis of the fluorescence intensities were shown in **K** (n = 3). **L,** Representative images of mitochondrial membrane potential detected by JC-1 fluorescent probe in H9c2 cells, and the quantitative analysis was established as the ratio of the JC-1 Monomers (Green) and JC-1 Aggregates (Red) in **M** (n = 3). **N–P,** Real-time oxygen consumption rates (OCR) and calculated basal and maximal respiration rates in H9c2 cells (n = 3). The data are presented as the Mean ± SD. *p < 0.05, **p < 0.01 and ***p < 0.001 vs. Vehicle group; #p < 0.05, ##p < 0.01, ###p < 0.001 vs. DOX group; ££p < 0.01 and £££p < 0.001 vs. DOX + NaHS group. (For interpretation of the references to colour in this figure legend, the reader is referred to the Web version of this article.)

persulfide group (R-S-S-H), has been identified as a novel post-translational modification by H_2S [35]. Recent advances have shown that H_2S regulated Keap1-Nrf2 signaling axis through Keap1 S-sulfhydration [28,29]. We next investigated the S-sulfhydration level of Keap1 using the "tag-switch" assay. The results showed that NaHS administration enhanced S-sulfhydration on Keap1, which significantly decreased in DOX-challenged cells (Fig. 8I and J).

Moreover, transfection with si*Cse* before DOX treatment resulted in a significant increase in the Nrf2/Keap1 interaction, a decreased protein level and nuclear translocation of Nrf2, a lower transcription level of SLC7A11 and GPx4 compared to the DOX group (Fig. 8K–R), due to the lack of Keap1 S-sulfhydration (Fig. 8S and T) but not the protein level of Keap1(Fig. 8K and N). All these can be partially reversed by NaHS administration (Fig. 8K–T). Collectively, these observations indicated that S-sulfhydration of Keap1 and the subsequent activation of Nrf2 are one of the key mechanisms to the protective effect of NaHS in DOX-induced cardiomyocyte ferroptosis.

4. Discussion

Various studies have already proposed that H_2S and its donors may offer a therapeutic approach for the prevention of DoIC. Wu et al. found that S-propargyl-cysteine (SPRC), a producing agent of endogenous H_2S, alleviated DOX-induced ROS production, mitochondrial dysfunction and intracellular Ca^{2+} overload by activating gp130-mediated STAT3 signaling [23]. Our previous study reported that H_2S reversed DOX-induced cardiac gap junction remodeling and then improved heart failure [21]. Other possible explanations for the protective effect of H_2S in DoIC included suppressing endoplasmic reticulum stress, cardiomyocyte apoptosis and autophagy [22,24]. Further, synthetic DOX derivatives conjugated with a H_2S-releasing moiety have been shown to be less cardiotoxic and more effective than the parent drug against P-glycoprotein overexpressing osteosarcoma cells [25].

In the present study, we focused on the role of H_2S in DOX-induced ferroptosis, a novel form of regulated cell death resulting from iron overload and accumulation of lipid peroxidation [36]. We detected and proved that DOX triggered ferroptosis in cardiomyocytes. Excess lipid peroxidation, one of the biochemical features of ferroptosis was observed in DoIC, as characterized by increased levels of MDA and *Ptgs2* mRNA. Mitochondria in cardiomyocytes displayed ferroptotic-like morphological changes, such as mitochondrial swelling and vacuolization with disintegration and lysis of cristae. Mitochondrial function was also impaired along with decreased mitochondrial membrane potential and respiration capacity. Meanwhile, in accordance with our previous study, we found the insufficiency of endogenous H_2S in DoIC [21]. CSE expression, its H_2S synthesizing activity and the level of H_2S in hearts were significantly suppressed by DOX both *in vivo* and *in vitro*. Application of exogenous H_2S significantly attenuated DOX-induced ferroptosis and improved the phenotype of DoIC. The protective effect of H_2S in DOX-induced ferroptosis could be mimicked by Fer-1, a ferroptosis inhibitor, but was significantly abrogated by pretreatment with Erastin2, a ferroptosis trigger. In contrast, further depletion of H_2S in cardiomyocyte-specific *Cse* deletion mice ($Cse^{f/f}$/Cre^{+}) or by *Cse* siRNA aggravated ferroptosis in DoIC and heart failure. The exacerbation could be partially reversed by supplementation of NaHS. These findings demonstrate the anti-ferroptosis role of H_2S in DoIC and encourage us to further explore the molecular mechanisms.

It is well-recognized that ferroptosis is mainly regulated by the competition between the ferroptosis execution system and the antioxidant defense system. SLC7A11/GSH/GPx4 signaling axis is one of the classic ferroptosis antioxidant pathways [10,27]. Extracellular cystine is imported into the cell through SLC7A11, and then converted to cysteine to synthesize GSH. GPx4 uses the reduced GSH as a co-factor to detoxify lipid peroxides to lipid alcohols, thereby preventing ferroptosis [10,37]. Here, we found that the expression of SLC7A11 and GPx4 along with the level of GSH were significantly suppressed in mice with DoIC or DOX-stimulated cardiomyocytes, eventually leading to excess lipid peroxidation, mitochondrial impairment and cell death. Interference with endogenous H_2S metabolism affected the activity of SLC7A11/GSH/GPx4 pathway in DoIC. Further inhibition of endogenous H_2S synthesis by cardiac *Cse* deletion or transfection with *Cse* siRNA in cardiomyocytes significantly downregulated the expression of SLC7A11 and GPx4 and augmented DOX-induced ferroptosis. Supplementation of exogenous H_2S in DoIC caused opposite effect on SLC7A11/GSH/GPx4 pathway. Further, using the Erastin2 to pharmacologically block SLC7A11, H_2S failed to exert its protective effect in DOX-induced cardiomyocyte ferroptosis. These findings highlight the involvement of SLC7A11/GSH/GPx4 signaling pathway in H_2S-mediated defense against DOX-induced ferroptosis.

To the best of our knowledge, it is the first study to show that H_2S attenuates ferroptosis and DOX-induced cardiac injury by upregulating the expression of system xÇ¯/GPx4 system. H_2S, dexrazoxane and Fer-1 remarkably relieved DOX-induced ferroptosis. However, they exert similar anti-ferroptosis effects via different mechanisms. Dexrazoxane fuses with free and bound iron, interferes Fenton reaction and decreases DOX-induced increase of cardiac nonheme iron [38–40]. H_2S combated DOX-induced ferroptosis and mitochondrial damage via stimulating SLC7A11/GSH/GPx4 pathway, but had no effect on iron accumulation in cardiomyocytes. Therefore, H_2S may have the potential to synergize with dexrazoxane and provide better protection in DoIC from diverse aspects.

Recently, H_2S has been suggested to post-translationally modify protein cysteine residues known as persulfidation or S-sulfhydration and regulate the function of target protein [13]. Thus, we speculated that upregulation of SLC7A11 and GPx4 expression by H_2S may be credited to persulfidation in Keap1-Nrf2-ARE (antioxidant response element) pathway, one of the most important regulators for antioxidant response in DOX challenged cardiomyocytes [41,42]. In our research, we found that H_2S persulfidated Keap1 and promoted Nrf2 nuclear translocation, which in turn promoted SLC7A11/GPx4 transcription through binding to the promoter containing ARE sequence and inhibited DOX-induced ferroptosis in cardiomyocytes. Other studies have observed that Keap-1 was inactivated by H_2S through persulfidating cysteine-151, cysteine-226 or cysteine-613 residues [28,29,43,44]. Moreover, independent of Keap1, H_2S activated the PI3K/AKT signaling pathway, increased the binding of Nrf2 to ARE and caused resistance to oxidative stress in rats with DOX-induced cardiomyopathy [24]. On the other hand, Fang et al. reported that DOX administration enhanced the nuclear accumulation of Nrf2, stimulated heme oxygenase (HO-1) expression and gave rise to the release of free iron and ferroptosis in

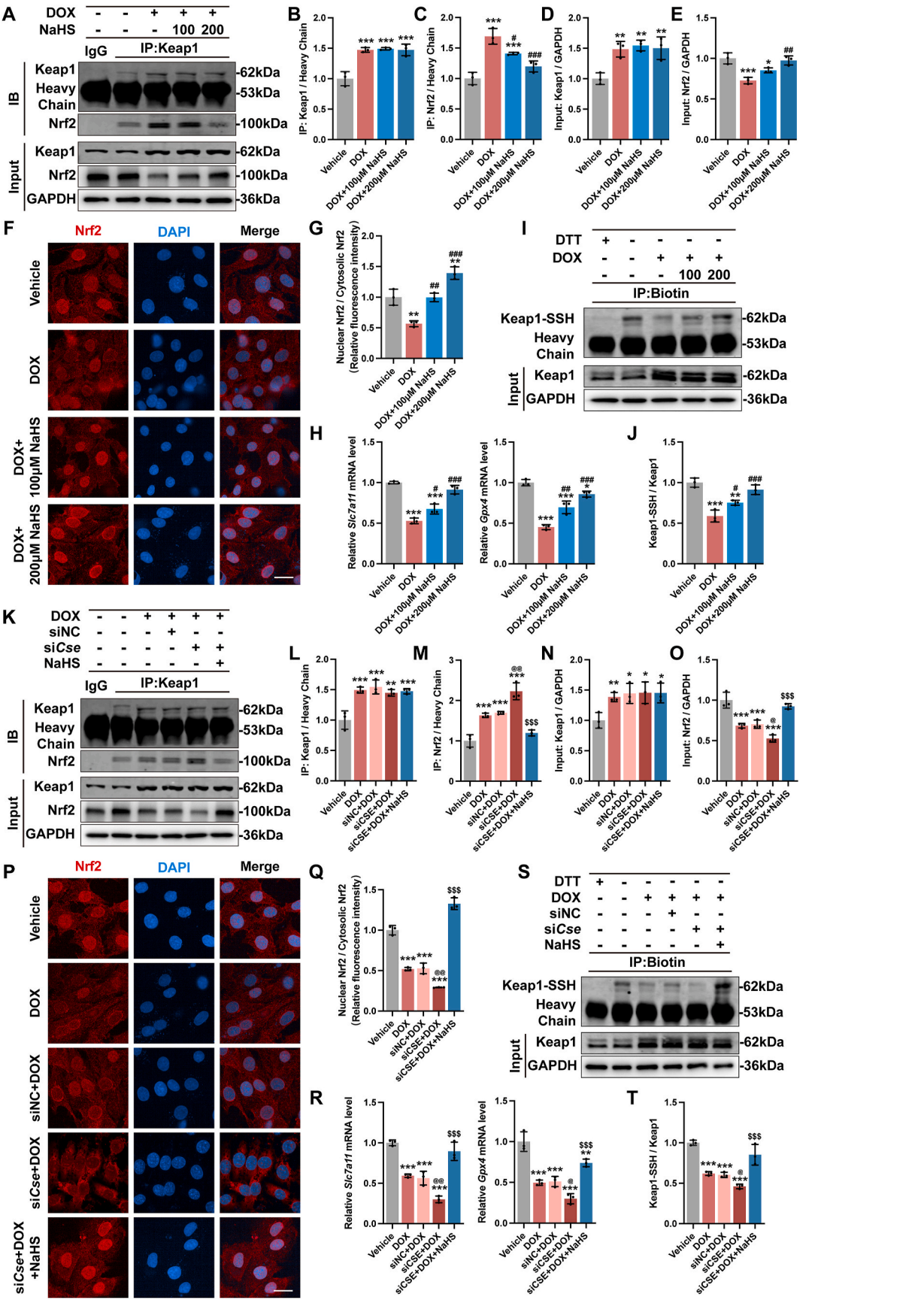

(caption on next page)

Fig. 8. H_2S promoted SLC7A11 and GPx4 transcription by inducing Keap1 S-sulfhydration and Nrf2 activation.
A-E, Cell lysates were immunoprecipitated with an anti-Keap1 or an anti-IgG antibody (negative control) and representative blots and quantitative analysis of Keap1 and Nrf2 protein levels (n = 3). **F,** Representative images of immunofluorescence staining of Nrf2 (Red) in H9c2 cells, and the quantitative analysis was established as the ratio of the nuclear Nrf2 and the cytosolic Nrf2 in **G** (n = 3). **H,** The expression levels of *Slc7a11 and Gpx4* mRNA in H9c2 cells (n = 3). **I** and **J,** S-sulfhydration on Keap1 was detected with the "tag-switch" method, representative blots and quantitative analysis of S-sulfhydrated Keap1 (Keap1-SSH) in H9c2 cells. **K–O,** Cell lysates were immunoprecipitated with an anti-Keap1 or an anti-IgG antibody (negative control) and representative blots and quantitative analysis of Keap1 and Nrf2 protein levels (n = 3). **P,** Representative images of immunofluorescence staining of Nrf2 (Red) in H9c2 cells, and the quantitative analysis was established as the ratio of the nuclear Nrf2 and the cytosolic Nrf2 in **Q** (n = 3). **R,** The expression levels of *Slc7a11 and Gpx4* mRNA in H9c2 cells (n = 3). **S** and **T,** S-sulfhydration on Keap1 was detected with the "tag-switch" method, representative blots and quantitative analysis of S-sulfhydrated Keap1 (Keap1-SSH) in H9c2 cells. The data are presented as the Mean ± SD. *p < 0.05, **p < 0.01 and ***p < 0.001 vs. Vehicle group; ##p < 0.01 and ###p < 0.001 vs. DOX group; @p < 0.05 and @@p < 0.01 vs. siNC + DOX group; $$$p < 0.001 vs. si*Cse* + DOX group. (For interpretation of the references to colour in this figure legend, the reader is referred to the Web version of this article.)

hearts [9]. The data seems conflicting to the anti-ferroptosis effect of Nrf2, as mentioned above, by activating the transcription of a set of anti-ferroptosis genes. Therefore, whether H_2S-mediated regulation of SLC7A11/GPx4 expression in DoIC is dependent on Keap1-Nrf2 signaling pathway warrants further investigation.

Of note, recent studies found that sulfane sulfur species (persulfides or polysulfides) are easily formed following the oxidation of endogenous H_2S by CSE/MPST in various tissues or by sulfur quinone oxidoreductase (SQR) in mitochondria [45–48]. Persulfides/polysulfides have been proposed to serve as a sink of endogenous H_2S and contribute to many of the biological effects currently attributed to H_2S [49]. Moreover, H_2S is theoretically difficult to react with protein thiol, because both molecules are in the same oxidation state (S atom in both H_2S and thiol is −2). Exogenous H_2S used in experiments that is mostly prepared by NaHS inevitably contains trace amounts of polysulfide. Therefore, it is possible that H_2S-related sulfane sulfur species rather than H_2S itself cause S-sulfhydration of cysteine residues. Indeed, some studies confirmed that endogenous persulfides/polysulfides in cells or tissues of mammals sulfurated cysteine residues and thus caused conformation changes in target protein to regulate their activity [45–48]. Taken together, H_2S may exert its effect on protein S-sulfhydration directly or by its derived sulfane sulfur species. Up to now, sulfane sulfur species are still understudied due to their inherent instability and lack of selective and sensitive detection methods. Their detailed mechanisms of biological action will be our future research direction.

Additionally, the analytical method of H_2S in our study is methylene blue assay. Due to the use of a strong acid in this method, H_2S can be easily released from acid-labile sulfur under a condition of a strong acid and its level is to some extent overestimated [50,51]. To get more insight in the roles of endogenous H_2S in DoIC and explore H_2S-based therapies, it is necessary to accurately measure the concentration of H_2S within biological systems. More reliable and sensitive methods, for example chromatography methods based on high performance liquid chromatography (HPLC) and gas chromatography will be used in our future study.

5. Conclusions

Our study demonstrated that loss of endogenous H_2S production aggravated the disruption of redox homeostasis and ultimately boosted DOX-induced cardiomyocyte ferroptosis. H_2S upregulated the activity of SLC7A11/GSH/GPx4 signaling pathway and defended against ferroptosis in DoIC by assisting GSH synthesis and alleviating lipid peroxidation due to the S-sulfhydration of Keap1 and the activation of Nrf2. Our findings provide a novel target in the application of H_2S to treat DOX-induced cardiac injury and heart failure.

Funding

This work was supported by Natural Science Foundation of Shanghai (Grant No. 21ZR1438000), National Natural Science Foundation of China (Grant No. 81570037) and Experimental Animal Research Project of Shanghai Science and Technology Commission (No.22140901200).

CRediT authorship contribution statement

Hui Zhang: Writing – original draft, Methodology, Investigation, Formal analysis, Data curation. **Jianan Pan:** Methodology, Investigation, Formal analysis, Data curation. **Shuying Huang:** Methodology, Investigation, Formal analysis, Data curation. **Xiaonan Chen:** Methodology, Data curation. **Alex Chia Yu Chang:** Resources, Methodology. **Changqian Wang:** Project administration, Methodology. **Junfeng Zhang:** Supervision, Project administration, Funding acquisition, Conceptualization. **Huili Zhang:** Writing – review & editing, Validation, Supervision, Project administration, Funding acquisition, Formal analysis, Data curation, Conceptualization.

Declaration of competing interest

The authors declare that they have no known competing financial interests or personal relationships that could have appeared to influence the work reported in this paper.

Data availability

No data was used for the research described in the article.

Appendix A. Supplementary data

Supplementary data to this article can be found online at https://doi.org/10.1016/j.redox.2024.103066.

References

[1] P.K. Singal, N. Iliskovic, Doxorubicin-induced cardiomyopathy, N. Engl. J. Med. 339 (1998) 900–905, https://doi.org/10.1056/NEJM199809243391307.
[2] B.E. Levis, P.F. Binkley, C.L. Shapiro, Cardiotoxic effects of anthracycline-based therapy: what is the evidence and what are the potential harms? Lancet Oncol. 18 (2017) e445–e456, https://doi.org/10.1016/S1470-2045(17)30535-1.
[3] A.R. Lyon, T. López-Fernández, L.S. Couch, R. Asteggiano, M.C. Aznar, J. Bergler-Klein, G. Boriani, D. Cardinale, R. Cordoba, B. Cosyns, D.J. Cutter, E. de Azambuja, R.A. de Boer, S.F. Dent, D. Farmakis, S.A. Gevaert, D.A. Gorog, J. Herrmann, D. Lenihan, J. Moslehi, B. Moura, S.S. Salinger, R. Stephens, T.M. Suter, S. Szmit, J. Tamargo, P. Thavendiranathan, C.G. Tocchetti, P. van der Meer, H.J.H. van der Pal, ESC Scientific document group, 2022 ESC guidelines on cardio-oncology developed in collaboration with the European hematology association (EHA), the European society for therapeutic radiology and oncology (ESTRO) and the international cardio-oncology society (IC-OS), Eur. Heart J. 43 (2022) 4229–4361, https://doi.org/10.1093/eurheartj/ehac244.
[4] Y. Octavia, C.G. Tocchetti, K.L. Gabrielson, S. Janssens, H.J. Crijns, A.L. Moens, Doxorubicin-induced cardiomyopathy: from molecular mechanisms to therapeutic strategies, J. Mol. Cell. Cardiol. 52 (2012) 1213–1225, https://doi.org/10.1016/j.yjmcc.2012.03.006.
[5] T. Km, R. Tc, Y. L, H. Bd, L. Lf, Adriamycin-induced DNA damage mediated by mammalian DNA topoisomerase II, Science 226 (1984), https://doi.org/10.1126/science.6093249.
[6] E. Christidi, L.R. Brunham, Regulated cell death pathways in doxorubicin-induced cardiotoxicity, Cell Death Dis. 12 (2021) 339, https://doi.org/10.1038/s41419-021-03614-x.
[7] J. Pan, W. Xiong, A. Zhang, H. Zhang, H. Lin, L. Gao, J. Ke, S. Huang, J. Zhang, J. Gu, A.C.Y. Chang, C. Wang, The imbalance of p53-Park7 signaling Axis induces iron homeostasis dysfunction in doxorubicin-challenged cardiomyocytes, Adv. Sci. Weinh. Baden-Wurtt. Ger. 10 (2023) e2206007, https://doi.org/10.1002/advs.202206007.

[8] T. Tadokoro, M. Ikeda, T. Ide, H. Deguchi, S. Ikeda, K. Okabe, A. Ishikita, S. Matsushima, T. Koumura, K. Yamada, H. Imai, H. Tsutsui, Mitochondria-dependent ferroptosis plays a pivotal role in doxorubicin cardiotoxicity, JCI Insight 5 (2020), https://doi.org/10.1172/jci.insight.132747.

[9] X. Fang, H. Wang, D. Han, E. Xie, X. Yang, J. Wei, S. Gu, F. Gao, N. Zhu, X. Yin, Q. Cheng, P. Zhang, W. Dai, J. Chen, F. Yang, H.-T. Yang, A. Linkermann, W. Gu, J. Min, F. Wang, Ferroptosis as a target for protection against cardiomyopathy, Proc. Natl. Acad. Sci. U. S. A. 116 (2019) 2672–2680, https://doi.org/10.1073/pnas.1821022116.

[10] N. Li, W. Jiang, W. Wang, R. Xiong, X. Wu, Q. Geng, Ferroptosis and its emerging roles in cardiovascular diseases, Pharmacol. Res. 166 (2021) 105466, https://doi.org/10.1016/j.phrs.2021.105466.

[11] H. Kimura, The physiological role of hydrogen sulfide and beyond, Nitric Oxide, Biol. Chem. 41 (2014) 4–10, https://doi.org/10.1016/j.niox.2014.01.002.

[12] X.-H. Yu, L.-B. Cui, K. Wu, X.-L. Zheng, F.S. Cayabyab, Z.-W. Chen, C.-K. Tang, Hydrogen sulfide as a potent cardiovascular protective agent, Clin. Chim. Acta Int. J. Clin. Chem. 437 (2014) 78–87, https://doi.org/10.1016/j.cca.2014.07.012.

[13] B.D. Paul, S.H. Snyder, H2S: a novel gasotransmitter that signals by sulfhydration, Trends Biochem. Sci. 40 (2015) 687–700, https://doi.org/10.1016/j.tibs.2015.08.007.

[14] R. Gupta, M. Sahu, R. Tripathi, R.K. Ambasta, P. Kumar, Protein S-sulfhydration: unraveling the prospective of hydrogen sulfide in the brain, vasculature and neurological manifestations, Ageing Res. Rev. 76 (2022) 101579, https://doi.org/10.1016/j.arr.2022.101579.

[15] B. Murphy, R. Bhattacharya, P. Mukherjee, Hydrogen sulfide signaling in mitochondria and disease, FASEB J. Off. Publ. Fed. Am. Soc. Exp. Biol. 33 (2019) 13098–13125, https://doi.org/10.1096/fj.201901304R.

[16] D.J. Polhemus, D.J. Lefer, Emergence of hydrogen sulfide as an endogenous gaseous signaling molecule in cardiovascular disease, Circ. Res. 114 (2014) 730–737, https://doi.org/10.1161/CIRCRESAHA.114.300505.

[17] S. Mani, H. Li, A. Untereiner, L. Wu, G. Yang, R.C. Austin, J.G. Dickhout, Š. Lhoták, Q.H. Meng, R. Wang, Decreased endogenous production of hydrogen sulfide accelerates atherosclerosis, Circulation 127 (2013) 2523–2534, https://doi.org/10.1161/CIRCULATIONAHA.113.002208.

[18] G. Yang, L. Wu, B. Jiang, W. Yang, J. Qi, K. Cao, Q. Meng, A.K. Mustafa, W. Mu, S. Zhang, S.H. Snyder, R. Wang, H2S as a physiologic vasorelaxant: hypertension in mice with deletion of cystathionine gamma-lyase, Science 322 (2008) 587–590, https://doi.org/10.1126/science.1162667.

[19] H. Zhang, L.-Z. Hao, J.-A. Pan, Q. Gao, J.-F. Zhang, R.K. Kankala, S.-B. Wang, A.-Z. Chen, H.-L. Zhang, Microfluidic fabrication of inhalable large porous microspheres loaded with H2S-releasing aspirin derivative for pulmonary arterial hypertension therapy, J. Control. Release Off. J. Control. Release Soc. 329 (2021) 286–298, https://doi.org/10.1016/j.jconrel.2020.11.060.

[20] S. Huang, X. Chen, J. Pan, H. Zhang, J. Ke, L. Gao, A.C. Yu Chang, J. Zhang, H. Zhang, Hydrogen sulfide alleviates heart failure with preserved ejection fraction in mice by targeting mitochondrial abnormalities via PGC-1α, Nitric Oxide, Biol. Chem. 136–137 (2023) 12–23, https://doi.org/10.1016/j.niox.2023.05.002.

[21] H. Zhang, A. Zhang, C. Guo, C. Shi, Y. Zhang, Q. Liu, A. Sparatore, C. Wang, S-diclofenac protects against doxorubicin-induced cardiomyopathy in mice via ameliorating cardiac gap junction remodeling, PLoS One 6 (2011) e26441, https://doi.org/10.1371/journal.pone.0026441.

[22] Z. Yu, W. Zhang, M. Zhang, M. Jin, W. Xu, X. Zhou, Gas signaling molecule hydrogen sulfide attenuates doxorubicin-induced dilated cardiomyopathy, Oncotarget 8 (2017) 95425–95431, https://doi.org/10.18632/oncotarget.20729.

[23] W. J, G. W, L. Sz, W. Zj, K. Jt, C. Sy, Z. Yz, Gp130-mediated STAT3 activation by S-propargyl-cysteine, an endogenous hydrogen sulfide initiator, prevents doxorubicin-induced cardiotoxicity, Cell Death Dis. 7 (2016), https://doi.org/10.1038/cddis.2016.209.

[24] L. Nie, M. Liu, J. Chen, Q. Wu, Y. Li, J. Yi, X. Zheng, J. Zhang, C. Chu, J. Yang, Hydrogen sulfide ameliorates doxorubicin-induced myocardial fibrosis in rats via the PI3K/AKT/mTOR pathway, Mol. Med. Rep. 23 (2021) 299, https://doi.org/10.3892/mmr.2021.11938.

[25] K. Chegaev, B. Rolando, D. Cortese, E. Gazzano, I. Buondonno, L. Lazzarato, M. Fanelli, C.M. Hattinger, M. Serra, C. Riganti, R. Fruttero, D. Ghigo, A. Gasco, H2S-Donating doxorubicins may overcome cardiotoxicity and multidrug resistance, J. Med. Chem. 59 (2016) 4881–4889, https://doi.org/10.1021/acs.jmedchem.6b00184.

[26] O. Kabil, R. Banerjee, Redox biochemistry of hydrogen sulfide, J. Biol. Chem. 285 (2010) 21903–21907, https://doi.org/10.1074/jbc.R110.128363.

[27] P. Koppula, L. Zhuang, B. Gan, Cystine transporter SLC7A11/xCT in cancer: ferroptosis, nutrient dependency, and cancer therapy, Protein Cell 12 (2021) 599–620, https://doi.org/10.1007/s13238-020-00789-5.

[28] S. Zhao, T. Song, Y. Gu, Y. Zhang, S. Cao, Q. Miao, X. Zhang, H. Chen, Y. Gao, L. Zhang, Y. Han, H. Wang, J. Pu, L. Xie, Y. Ji, Hydrogen sulfide alleviates liver injury through the S-Sulfhydrated-Kelch-Like ECH-associated protein 1/nuclear Erythroid 2-related factor 2/low-density lipoprotein receptor-related protein 1 pathway, Hepatol. Baltim. Md. 73 (2021) 282–302, https://doi.org/10.1002/hep.31247.

[29] L. Xie, Y. Gu, M. Wen, S. Zhao, W. Wang, Y. Ma, G. Meng, Y. Han, Y. Wang, G. Liu, P.K. Moore, X. Wang, H. Wang, Z. Zhang, Y. Yu, A. Ferro, Z. Huang, Y. Ji, Hydrogen sulfide induces Keap1 S-sulfhydration and suppresses diabetes-accelerated atherosclerosis via Nrf2 activation, Diabetes 65 (2016) 3171–3184, https://doi.org/10.2337/db16-0020.

[30] X. Chen, H. Lin, W. Xiong, J. Pan, S. Huang, S. Xu, S. He, M. Lei, A.C.Y. Chang, H. Zhang, p53-Dependent mitochondrial compensation in heart failure with preserved ejection fraction, J. Am. Heart Assoc. 11 (2022) e024582, https://doi.org/10.1161/JAHA.121.024582.

[31] L. Li, M. Bhatia, Y.Z. Zhu, Y.C. Zhu, R.D. Ramnath, Z.J. Wang, F.B.M. Anuar, M. Whiteman, M. Salto-Tellez, P.K. Moore, Hydrogen sulfide is a novel mediator of lipopolysaccharide-induced inflammation in the mouse, FASEB J. Off. Publ. Fed. Am. Soc. Exp. Biol. 19 (2005) 1196–1198, https://doi.org/10.1096/fj.04-3583fje.

[32] Z. Li, Q. Duan, Y. Cui, O.D. Jones, D. Shao, J. Zhang, Y. Gao, X. Cao, S. Wang, J. Li, X. Lei, W. Zhang, L. Wang, X. Zhou, M. Xu, Y. Liu, J. Ma, X. Xu, Cardiac-specific expression of cre recombinase leads to age-related cardiac dysfunction associated with tumor-like growth of atrial cardiomyocyte and ventricular fibrosis and ferroptosis, Int. J. Mol. Sci. 24 (2023) 3094, https://doi.org/10.3390/ijms24043094.

[33] J.Y. Cao, A. Poddar, L. Magtanong, J.H. Lumb, T.R. Mileur, M.A. Reid, C.M. Dovey, J. Wang, J.W. Locasale, E. Stone, S.P.C. Cole, J.E. Carette, S.J. Dixon, A genome-wide haploid genetic screen identifies regulators of glutathione abundance and ferroptosis sensitivity, Cell Rep. 26 (2019) 1544–1556.e8, https://doi.org/10.1016/j.celrep.2019.01.043.

[34] S.J. Dixon, D.N. Patel, M. Welsch, R. Skouta, E.D. Lee, M. Hayano, A.G. Thomas, C. E. Gleason, N.P. Tatonetti, B.S. Slusher, B.R. Stockwell, Pharmacological inhibition of cystine-glutamate exchange induces endoplasmic reticulum stress and ferroptosis, Elife 3 (2014) e02523, https://doi.org/10.7554/eLife.02523.

[35] S.-I. Bibli, I. Fleming, Oxidative post-translational modifications: a focus on cysteine S-sulfhydration and the regulation of endothelial fitness, antioxid, Redox Signal 35 (2021) 1494–1514, https://doi.org/10.1089/ars.2021.0162.

[36] S.J. Dixon, K.M. Lemberg, M.R. Lamprecht, R. Skouta, E.M. Zaitsev, C.E. Gleason, D.N. Patel, A.J. Bauer, A.M. Cantley, W.S. Yang, B. Morrison, B.R. Stockwell, Ferroptosis: an iron-dependent form of nonapoptotic cell death, Cell 149 (2012) 1060–1072, https://doi.org/10.1016/j.cell.2012.03.042.

[37] S.C. Lu, Regulation of glutathione synthesis, Mol. Aspect. Med. 30 (2009) 42–59, https://doi.org/10.1016/j.mam.2008.05.005.

[38] Y. QuanJun, Y. GenJin, W. LiLi, H. YongLong, H. Yan, L. Jie, H. JinLu, L. Jin, G. Run, G. Cheng, Protective effects of dexrazoxane against doxorubicin-induced cardiotoxicity: a metabolomic study, PLoS One 12 (2017) e0169567, https://doi.org/10.1371/journal.pone.0169567.

[39] S.M. Swain, P. Vici, The current and future role of dexrazoxane as a cardioprotectant in anthracycline treatment: expert panel review, J. Cancer Res. Clin. Oncol. 130 (2004) 1–7, https://doi.org/10.1007/s00432-003-0498-7.

[40] J.C. Kwok, D.R. Richardson, The cardioprotective effect of the iron chelator dexrazoxane (ICRF-187) on anthracycline-mediated cardiotoxicity, Redox Rep. Commun. Free Radic. Res. 5 (2000) 317–324, https://doi.org/10.1179/135100000101535898.

[41] H. K, S. J, Y. J, Z. C, Z. J, P. Ja, Z. Y, J. Y, W. Y, L. Rz, C. H, G. S, Z. Wx, Loss of TRIM21 alleviates cardiotoxicity by suppressing ferroptosis induced by the chemotherapeutic agent doxorubicin, EBioMedicine 69 (2021), https://doi.org/10.1016/j.ebiom.2021.103456.

[42] K.K.S. Nordgren, K.B. Wallace, Disruption of the Keap1/Nrf2-antioxidant response system after chronic doxorubicin exposure in vivo, Cardiovasc. Toxicol. 20 (2020) 557–570, https://doi.org/10.1007/s12012-020-09581-7.

[43] J.M. Hourihan, J.G. Kenna, J.D. Hayes, The gasotransmitter hydrogen sulfide induces nrf2-target genes by inactivating the keap1 ubiquitin ligase substrate adaptor through formation of a disulfide bond between cys-226 and cys-613, Antioxid, Redox Signal 19 (2013) 465–481, https://doi.org/10.1089/ars.2012.4944.

[44] G. Yang, K. Zhao, Y. Ju, S. Mani, Q. Cao, S. Puukila, N. Khaper, L. Wu, R. Wang, Hydrogen sulfide protects against cellular senescence via S-sulfhydration of Keap1 and activation of Nrf2, Antioxidants Redox Signal. 18 (2013) 1906–1919, https://doi.org/10.1089/ars.2012.4645.

[45] T. Ida, T. Sawa, H. Ihara, Y. Tsuchiya, Y. Watanabe, Y. Kumagai, M. Suematsu, H. Motohashi, S. Fujii, T. Matsunaga, M. Yamamoto, K. Ono, N.O. Devarie-Baez, M. Xian, J.M. Fukuto, T. Akaike, Reactive cysteine persulfides and S-polythiolation regulate oxidative stress and redox signaling, Proc. Natl. Acad. Sci. U. S. A. 111 (2014) 7606–7611, https://doi.org/10.1073/pnas.1321232111.

[46] Y. Kimura, Y. Mikami, K. Osumi, M. Tsugane, J. Oka, H. Kimura, Polysulfides are possible H2S-derived signaling molecules in rat brain, FASEB J. Off. Publ. Fed. Am. Soc. Exp. Biol. 27 (2013) 2451–2457, https://doi.org/10.1096/fj.12-226415.

[47] H. Kimura, Signaling molecules: hydrogen sulfide and polysulfide, Antioxidants Redox Signal. 22 (2015) 362–376, https://doi.org/10.1089/ars.2014.5869.

[48] N. Nagahara, S. Koike, T. Nirasawa, H. Kimura, Y. Ogasawara, Alternative pathway of H2S and polysulfides production from sulfurated catalytic-cysteine of reaction intermediates of 3-mercaptopyruvate sulfurtransferase, Biochem. Biophys. Res. Commun. 496 (2018) 648–653, https://doi.org/10.1016/j.bbrc.2018.01.056.

[49] H. Kimura, Signalling by hydrogen sulfide and polysulfides via protein S-sulfuration, Br. J. Pharmacol. 177 (2020) 720–733, https://doi.org/10.1111/bph.14579.

[50] N.L. Whitfield, E.L. Kreimier, F.C. Verdial, N. Skovgaard, K.R. Olson, Reappraisal of H2S/sulfide concentration in vertebrate blood and its potential significance in ischemic preconditioning and vascular signaling, Am. J. Physiol. Regul. Integr. Comp. Physiol. 294 (2008) R1930–R1937, https://doi.org/10.1152/ajpregu.00025.2008.

[51] M. Ishigami, K. Hiraki, K. Umemura, Y. Ogasawara, K. Ishii, H. Kimura, A source of hydrogen sulfide and a mechanism of its release in the brain, Antioxidants Redox Signal. 11 (2009) 205–214, https://doi.org/10.1089/ars.2008.2132.